Measuring Livestock from Space: Global and U.S. Evidence on the Detection, Attribution, and Limits of Satellite Methane*

Jianwei Ai Qinan Lu Wendong Zhang

October 27, 2026

Abstract

Livestock are difficult to measure consistently in areas with sparse agricultural statistics. This paper examines the potential and limitations of using satellite-derived methane measurements to assess livestock activity. Combining global 0.1° methane observations with gridded livestock data from 2003 to 2020, we find that nearby areas with more livestock have higher methane concentrations. The relationship survives controls for competing methane sources and does not appear for pollutants that livestock do not emit. Yet the signal has clear limits. Satellite methane does not reliably track local changes in herd size over time, and because herd locations persist, it adds little to predicting herd size once a location's coordinates are known. Detectability depends on whether livestock emissions are large and concentrated enough to stand out against the local methane background. In the United States, satellite methane tracks concentrated dairy cattle but not dispersed beef cattle, and California cells with large dairy facilities show higher methane concentrations. Satellite methane is therefore a useful tool for screening and independently verifying large, concentrated operations, and filling facility-level monitoring gaps in countries where official statistics are sparse or outdated.

Keywords: Livestock; Methane; Remote Sensing; Agricultural Measurement; Detection Envelope; Dairy Cattle; Beef Cattle; CAFO; Climate Change

JEL Codes: Q12, Q52, Q53, C81, H23

*Ai: Cornell University (email: jianwei.ai@cornell.edu); Lu: Peking University (email: qinan.lu@pku.edu.cn); Zhang: Cornell University (email: wendongz@cornell.edu).

Acknowledgments: We thank participants from various seminars and conferences for helpful comments. Zhang gratefully acknowledges gifts to the Environmental Defense Fund and the Cornell Atkinson Center for Sustainability from the David and Patricia Atkinson Foundation. All remaining errors are our own.

Conflicts of Interest: The authors declare no ties to the agricultural industry and no other conflicts of interest. This paper has not been accepted for publication and is not scheduled to be published before the conference date.

1 Introduction

Reliable measures of livestock activity remain scarce in many parts of the world, limiting efforts to monitor agricultural production and its environmental consequences (Davis et al., 2025). Existing livestock statistics rely primarily on censuses and surveys that are costly to administer, conducted infrequently, and uneven in their spatial coverage and quality. These limitations are particularly consequential for livestock, which account for roughly 40 percent of the global value of agricultural output, occupies about a quarter of the Earth's ice-free land through grazing, and produces roughly a third of anthropogenic methane emissions (Gerber et al., 2013; Xu et al., 2021; Saunois et al., 2025). Even where official statistics are available, inventories are often reported at administrative or size thresholds that obscure substantial variation in the location and concentration of production. Measuring livestock activity more consistently and at finer spatial scales would therefore improve the assessment of environmental impacts of livestock production. These limitations create demand for independent, spatially consistent measures of livestock activity that do not rely solely on producer reporting.

Satellite methane observations offer a potential source of such information because livestock activity generates methane emissions that can be observed from space (Jacob et al., 2016; Parker et al., 2020). Yet atmospheric methane is not a direct measure of livestock activity. Livestock numbers first translate into emissions, which then disperse through the atmosphere before appearing in satellite measurements of column methane concentrations. The strength and detectability of this signal vary across locations and production systems. Emissions differ across animal species and manure-management practices (Intergovernmental Panel on Climate Change, 2006; Gerber et al., 2013), while the spatial concentration of production, atmospheric transport, and terrain determine how strongly these emissions appear in satellite observations (Jacob et al., 2016). Even when livestock emissions are detectable, distinguishing them from other methane sources remains challenging. Satellites also observe methane from wetlands, fossil fuels, waste, rice cultivation, and other sources, which can obscure the livestock signal (Saunois et al., 2025). These challenges raise a broader question of whether detecting methane associated with livestock activity can provide useful information about livestock production.

We examine this question by distinguishing three dimensions of satellite-based livestock measurement. First, can satellites detect methane emissions associated with livestock activity? Second, when can this signal recover information about livestock activity itself? Third, does satellite methane add anything beyond what existing agricultural statistics and geography already reveal? Answering these questions addresses a significant gap in agricultural economic statistics, particularly for countries where livestock methane relies on models rather than observed facility-level data. These distinctions separate three concepts that are often implicitly treated as equivalent. Detecting methane associated with livestock does not necessarily imply that satellite observations can recover livestock inventories, and recovering a spatial livestock signal does not necessarily imply that satellites improve on existing information. Establishing where these links hold (and where they break down) is therefore necessary for assessing the statistical value of satellite methane. We

address these questions by combining global satellite observations with livestock inventories and administrative records at finer spatial scales.

We begin by testing whether satellite methane contains a detectable spatial signal of livestock activity at the global scale. We combine global 0.1° satellite-based methane concentrations from GHAP with gridded livestock inventories from the Annual Gridded Livestock of the World (AGLW) dataset for 2003–2020 Du et al. (2025). Our baseline specification compares grid cells within 5° × 5° neighborhoods, absorbing broad spatial differences in atmospheric conditions and methane backgrounds. Within the same neighborhood, cells with greater livestock activity have systematically higher methane concentrations. The relationship is positive on five of six continents and is robust to alternative measures of livestock activity based on animal counts rather than predicted emissions. These results establish a persistent spatial association between livestock activity and satellite methane, but they do not by themselves show that the observed signal reflects livestock rather than other correlated methane sources or environmental conditions.

We next test whether this spatial relationship reflects livestock emissions. Controlling for methane emissions from rice cultivation, fossil fuels, and waste leaves the livestock relationship largely unchanged. We then conduct placebo tests using satellite-based ozone and column carbon dioxide, pollutants that respond to atmospheric transport and economic activity but are not directly produced by livestock methane emissions. Livestock activity predicts methane far more strongly than ozone. Column carbon dioxide also rises with livestock, but controlling for it leaves about 60 percent of the methane coefficient, the share specific to methane. The relationship is also stronger where methane is elevated relative to carbon dioxide, a pattern more consistent with biogenic than fossil sources. These tests support interpreting the spatial gradient as a livestock-related methane signal rather than a general feature of livestock-producing locations.

The satellite signal, however, is not uniformly informative about livestock activity and has two main limitations. First, out-of-sample classification exercises reveal substantial differences in detectability across countries. Satellite methane identifies livestock-intensive areas well in the United States but performs much less reliably in other regions such as Australia, where livestock emissions are more dispersed or competing methane sources are important. Second, Second, the signal does not extend to changes over time. Methane captures persistent cross-sectional differences in livestock activity but does not reliably track local changes in herd size over time. These patterns define a detection envelope in which satellite methane is most informative when livestock emissions are sufficiently large and spatially concentrated relative to the local methane background.

Finally, we use much finer-scale U.S. administrative data to confirm this detection envelope and clarify the statistical value of satellite methane. U.S. administrative data reveal a similar distinction across production systems. Satellite methane tracks dairy cattle, which are concentrated in large operations with substantial manure emissions, but is much less informative about geographically dispersed beef cattle, whose methane is almost entirely enteric and whose manure share is 2 percent (Food and Agriculture Organization of the United Nations, 2024). Within California's Central Valley, grid cells containing large dairy facilities have higher methane concentrations than other

cells in the same county, and the difference remains after controlling for column carbon dioxide from the same instrument, which absorbs the mechanical effect of terrain on any column measurement: a column average reads lower over high ground because methane-poor upper air makes up more of a shorter column. Satellite methane adds little to predicting continuous herd size once a model includes geographic coordinates: herd locations persist over time, so location alone predicts the count, and the column raises out-of-sample accuracy by only 0.004 in R^2. It is more informative as a detector, raising the hit rate for flagging exceptionally large livestock concentrations from 12.8 to 19.2 percent.

Our paper contributes to three strands of literature. First, we contribute to a growing literature that uses remotely sensed data to measure economic activity when conventional statistics are limited (Henderson et al., 2012; Donaldson and Storeygard, 2016; Jean et al., 2016; Yang et al., 2025; Rossi-Hansberg and Zhang, 2026; Wuepper et al., 2025). We assess satellite methane as a measure of livestock activity worldwide, across countries whose livestock records differ widely in detail. This strand of literature has shown that satellite observables can recover information about outcomes ranging from economic activity and poverty to agricultural production. Our setting highlights a distinct measurement problem. The physical signal observed by a satellite need not map one-to-one into the underlying economic activity of interest. Livestock activity must first generate emissions, those emissions must produce a sufficiently concentrated atmospheric signal, and that signal must be distinguishable from other methane sources before it becomes informative in satellite observations. We characterize this mapping empirically and show that its reliability varies systematically across production systems and methane environments. Testing it globally matters because the United States, where county records make validation possible, is where the measure adds least to existing statistics; the cross-country results show that it transfers to China and India, whose herd records are coarser, but not to the dispersed herds of Australia or to Brazil, where wetlands dominate local methane. The results therefore move the question from whether a remotely sensed variable proxies for economic activity on average to the conditions under which it is informative, which requires mapping the detection envelope of a measure as well as its average predictive performance.

Second, we contribute to the literature that uses atmospheric observations to measure and attribute methane emissions (Jacob et al., 2016; Duren et al., 2019; Lauvaux et al., 2022; Worden et al., 2023; East et al., 2025; Hancock et al., 2025). Existing work has demonstrated the value of satellite observations for detecting large methane sources, quantifying regional and national emissions, and evaluating bottom-up inventories. Recent controlled-release experiments provide direct evidence of these capabilities. In a year-long study that compared satellite observations with known methane releases, instruments specifically designed to detect methane identified 92–100 percent of releases under clear-sky conditions, while other instruments performed less reliably (Reuland et al., 2026). We approach the measurement problem from the opposite direction: starting from independently measured livestock activity, we ask when its atmospheric signature can be recovered from satellite methane. This approach helps explain why concentrated dairy production leaves a detectable satellite signature while dispersed livestock systems often do not, and why the

same satellite measure performs differently across methane environments.

Third, we contribute to work on agricultural statistics by clarifying the comparative advantage of satellite-based measures (Lobell, 2013; Davis et al., 2025; Wuepper et al., 2025; Proctor et al., 2025). Remote sensing can provide spatially consistent information without relying on producer reporting, making it potentially valuable where conventional agricultural data are sparse, infrequent, or difficult to verify. The two systems can also disagree: satellite- and survey-based crop yields diverge systematically, most where statistical capacity is weakest, so conclusions that depend on agricultural data can turn on the choice of measurement system (Park et al., 2026). Our results also show why this advantage should not be interpreted as implying that satellite measures can replace conventional statistics. Satellite methane adds little to continuous herd-size prediction once geographic information is known and does not reliably recover local changes in livestock inventories over time. In the United States, it also tracks dairy cattle rather than beef, so where herd composition is unrecorded it can indicate where concentrated dairying is likely. Its comparative advantage instead lies in providing an independent physical signal of unusually large and concentrated livestock activity. Satellite methane can therefore complement, rather than substitute for, conventional livestock statistics by screening locations where official data are limited and providing independent verification where concentrated activity is expected to generate a detectable atmospheric signal.

The remainder of the paper is organized as follows. Section 2 describes the satellite methane, livestock, and validation data. Section 3 presents the empirical framework for spatial validation, detection, and prediction. Section 4 establishes the global livestock-related methane signal and assesses its attribution using competing methane sources and atmospheric placebo tests. Section 5 examines when this signal is informative about livestock activity, focusing on variation across methane environments and production systems, facility-level validation, and the incremental information provided by satellite methane. Section 6 discuss the implications of our findings, and Section 7 concludes.

2 Data and Measurement

Our analysis combines global satellite methane observations with gridded livestock inventories, other methane sources, and U.S. administrative and facility-level records. Satellite carbon dioxide and ozone are used for attribution and placebo tests. This section describes the satellite methane measure, livestock activity and emissions, and the additional data used for attribution and validation.

2.1 Satellite Methane

Our satellite measure comes from the GlobalHighAirPollutants (GHAP) column methane product developed by Qu et al. (2025), a daily, spatially complete 0.1° record of the column-averaged dry-air mole fraction of methane (XCH_4) over land for 2003 to 2020. XCH_4 measures atmospheric methane concentration in parts per billion (ppb) of dry air. GHAP fuses two satellite retrievals,

SCIAMACHY for 2003 to 2009 and GOSAT for 2010 to 2020. Where soundings are missing, a spatiotemporal Transformer model predicts XCH_4 from the CAMS methane reanalysis, its leading input, together with meteorological variables, vegetation indices, and terrain, and the full field is then bias-corrected against the Total Carbon Column Observing Network (TCCON) ground stations, a global network of ground-based spectrometers that provides the reference standard for column measurements. The fused product reaches an R^2 of 0.93 against TCCON with a root-mean-square error of 13.1 ppb, and cross-validated accuracy after bias correction is R^2 of 0.95 to 0.97 with errors of 7.5 to 9.6 ppb (Qu et al., 2025). Because these daily errors are an order of magnitude larger than the livestock signal we estimate, our design never interprets a single cell-day: we average the daily fields to annual grid-cell means and identify from differences within 5° neighborhoods. Section 6 discusses what the reanalysis-assisted reconstruction implies for interpretation.[1] Our primary outcome is raw XCH_4. Across grid cells with livestock data in 2020, mean XCH_4 is approximately 1,848 ppb, with a cross-sectional standard deviation of 21 ppb, as illustrated in Appendix Table A3.

Column methane has risen rapidly over the sample period, as Figure 1 shows. Column methane is higher in the Northern Hemisphere than the Southern Hemisphere and peaks over the major continental source regions, most visibly East and South Asia, where dense agriculture, wetlands, and industry coincide. Between 2003 and 2020, the concentration rose almost everywhere, consistent with the documented global increase in atmospheric methane (Saunois et al., 2025). Because observed column methane combines local emissions with broad atmospheric background and transport, livestock-related variation represents only one component of the observed concentration. Appendix Figure A1 summarizes the methane concentration by region and year.

2.2 Global Livestock Activity and Methane Emissions

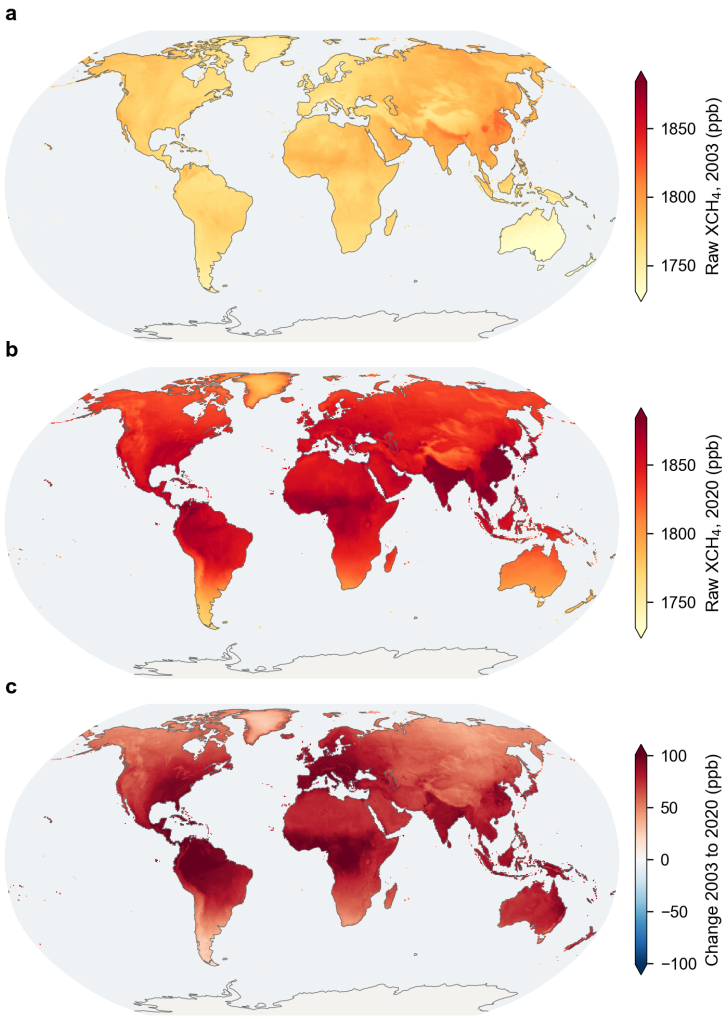
Livestock activity comes from the Annual Gridded Livestock of the World (AGLW) dataset compiled by Du et al. (2025), which provides annual animal density at 0.1° resolution from 1961 to 2021 across the globe for the six animal types that are most relevant enteric and manure methane: cattle, buffaloes, sheep, goats, pigs, and poultry. We convert species-specific densities to head counts using grid-cell area. Aggregated globally, the gridded product matches Food and Agriculture Organization (FAO) census head counts closely.[2]

The spatial composition of the herd is shifting, and the shift is regional. Globally, livestock changed in three ways from 2003 to 2020, as Figure 2 presents. Cattle density grew across the Sahel, the East African highlands, and South and Central Asia, and fell across Europe, the Russian steppe, and parts of Australia. Goat density grew over much of the same ground, and more strongly. Additionally, the small ruminant share of the ruminant herd rose across Central Asia, the Sahel, and southern Africa, and fell across parts of South America and Southeast Asia. Every species'

[1] Appendix Table A2 summarizes the data sources, coverage, resolution, and role in the analysis.

[2] For example, 1.51 billion cattle in 2020 against an FAO figure near 1.53 billion, and 0.94 billion pigs against about 0.95 billion, which supports its use as an activity measure.

Figure 1. Raw column methane, 2003, 2020, and change



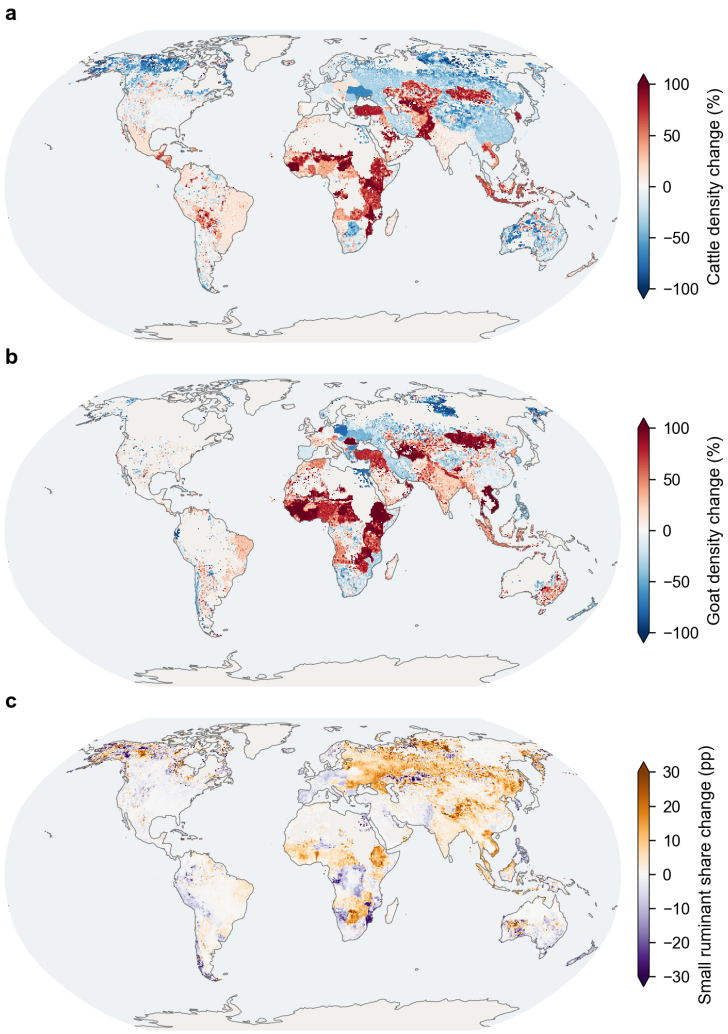
Notes: GHAP XCH_4 in parts per billion (ppb) on a fixed color scale. The figure shows the raw column methane concentration using GHAP in 2003 and 2020 and the change between them. Source: GHAP.

headcount trended upward over 2003–2020, with the fastest proportional growth in poultry and goats and slower growth in cattle and pigs (Appendix Figure A2).

Our baseline measure converts livestock headcounts into predicted methane emissions using IPCC 2006 Tier 1 emission factors (Intergovernmental Panel on Climate Change, 2006).[3] These factors differ by more than two orders of magnitude across species, so livestock head counts and predicted methane emissions can differ substantially in their spatial distribution. Appendix Figure A3 links the headcount with methane emission and maps the species that contribute the most Tier 1 methane in each cell. Cattle dominate the Americas, much of Africa, and South Asia, buffaloes

[3]Tier 1 factors are the IPCC's default per-head emission rates, which differ by more than two orders of magnitude across species. The annual factors for cattle, buffaloes, sheep, goats, pigs, and poultry are 62, 55, 8, 5, 1.5, and 0.02 kilograms of CH_4 per head, respectively, combining enteric fermentation and manure management.

Figure 2. Change in livestock density

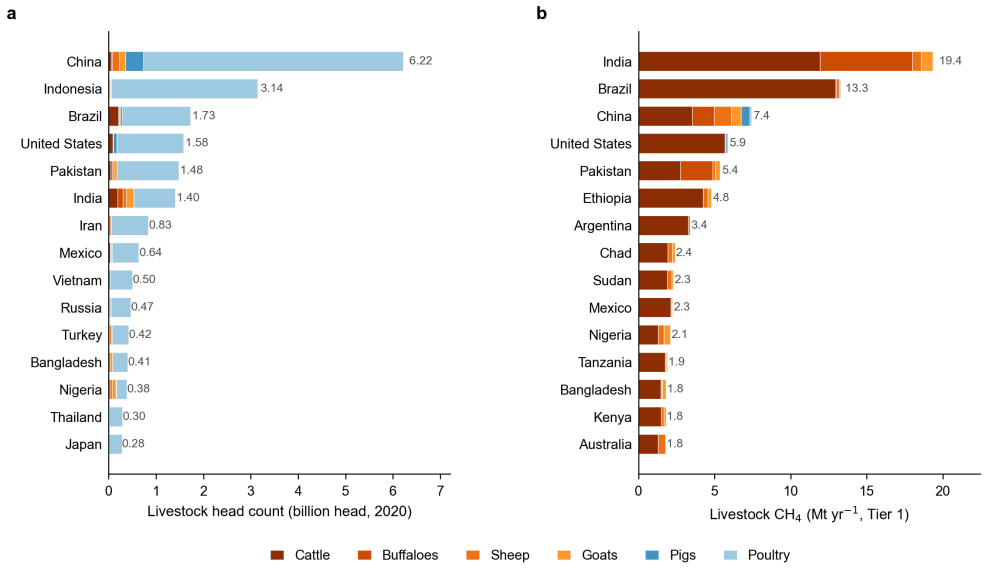


Notes: Change from 2003 to 2020 in (a) cattle density, (b) goat density, both as a percent of the 2003 level and clipped at plus or minus one hundred percent, and (c) the small ruminant share of the ruminant herd, in percentage points. Cattle and goats grew together across the Sahel, East Africa, and South and Central Asia and declined across Europe and the Russian steppe; the composition panel shows where that growth tilted the herd toward goats and sheep. Cells with negligible livestock are left blank. Source: AGLW.

dominate the Indo-Gangetic Plain, and small ruminants dominate the Sahel and Central Asia. This spatial heterogeneity is one reason the livestock methane relationship need not be homogeneous, which motivates estimating it separately by region.

Figure 3 shows that China leads on headcount at 6.2 billion animals but falls to third on methane at 7.4 megatons, because a chicken emits about one three-thousandth, and a pig about one fortieth, of a cow's methane per head, while India and Brazil, with large ruminant herds, lead on methane at 19.4 and 13.3 megatons. The headcount panel is dominated by poultry and the methane panel by cattle and buffalo, with the three largest emitters together accounting for about a third of the global total.

Figure 3. Weighting animals by what they emit reverses the country ranking



Notes: Top fifteen countries in 2020 by (a) total livestock head count and (b) Tier 1 livestock methane, both stacked by species and computed from the same area-weighted gridded census. China leads on head count but ranks third on methane, while India and Brazil lead on methane. Source: AGLW with IPCC Tier 1 factors.

2.3 Other Methane Sources and Validation Data

Rice paddy, fossil fuel, and waste. We use gridded measures of rice cultivation, fossil-fuel methane, and waste methane to account for major non-livestock methane sources. Rice paddy extent comes from the GlobalRice20 product, a 20-meter binary paddy mask that we aggregate to a 0.1° rice fraction by averaging fine-resolution pixels within each grid cell. Because paddy extent is relatively stable over our study period, we use the 2015 layer as a near-static confounder.

We measure fossil-fuel and waste methane directly using sector-specific gridded inventories. Fossil methane comes from the Global Fuel Exploitation Inventory (Scarpelli et al., 2022), a 0.1° inventory that allocates national oil, gas, and coal methane to infrastructure locations. We sum its oil, gas, and coal layers into a single fossil grid. Waste methane comes from the EDGAR v2025 sector split grids for solid waste landfills and for wastewater, which we similarly combine into a single waste grid. Because the location of oil and gas fields, coal mines, and landfills is spatially stable over our period, we treat both layers as near-static confounders, as we do for rice, using the GFEI reference year and the 2020 EDGAR waste layer.

Placebo pollutants. We use CO_2 and O_3 as placebo outcomes because both co-move with general economic activity and share the instrument and retrieval pipeline, but are not produced by livestock. Column carbon dioxide (XCO_2) comes from GHAP and is observed on the same 0.1° grid and over the same period as XCH_4, providing a closely matched atmospheric comparison. Surface ozone comes from the GHAP global seamless ozone product, also at 0.1° and on the identical grid,

for which we use the 2019 layer to match the analysis year.

Neither pollutant should exhibit the same spatial relationship with livestock as methane. Ruminants do respire carbon dioxide, but that carbon was fixed by the plants they ate and returns on a short cycle, so it does not accumulate in the column as fossil carbon does. Ozone is a secondary pollutant formed photochemically from precursors livestock do not emit. A livestock gradient in either would therefore point to our regressor proxying for something other than livestock methane. We merge both to the panel grid cell by cell and restrict the placebo sample analysis to cells in which all three pollutants are observed.

United States ground-truth and market validation data. We use the US to validate the satellite signal against independent livestock records at finer spatial scales. For the United States application, we use five public sources. First, USDA NASS QuickStats provides state and national cattle and hog inventory, which we obtain from the bulk data files. Second, the Bureau of Labor Statistics provides monthly producer and consumer price indices for cattle, hogs, beef, pork, and dairy from 2003 to 2020. Third, FAOSTAT provides Tier 1 livestock methane by country and species, split into enteric fermentation and manure management, and separating dairy from non-dairy cattle. We use the FAOSTAT split to characterize the concentrated manure channel that distinguishes detectable from undetectable operations.

The fourth source is the county-by-year panel of USDA cattle inventories, covering 2000 to 2024 and reporting milk cattle and beef cattle as separate series. We use it to distinguish the two herds at a spatial resolution the state data cannot reach. Satellite methane also lets us separate dairy from beef, which the global grid alone cannot. We match the state cross-section using the 2017 census year.

Last, we use a facility-level point file of confined animal feeding operations with coordinates, production type, and animal population for 37,841 facilities. We assign each 0.1° cell to a county by point-in-polygon overlay and distribute each county's dairy and beef herd uniformly across its cells, which is a strong assumption we return to when interpreting the estimates.

3 Methodology

We frame the analysis as a measurement validity problem. The object of interest is whether a satellite signal, column methane, tracks an economic quantity and livestock activity. In this section, we first present an empirical design to show the linear correlation through a linear regression, and then use various machine learning models to detect non-linear relationships between livestock and methane emission, considering all kinds of confounders.

3.1 Regression-Based Spatial Validation Design

Let y_i be raw XCH_4 in grid cell i, and let ℓ_i be Tier 1 livestock methane in that cell, area weighted. We estimate

$$y_i = \beta \log \ell_i + \alpha_{n(i)} + \varepsilon_i, \tag{1}$$

where $\alpha_{n(i)}$ is a fixed effect for the 5° by 5° neighborhood $n(i)$ that contains cell i. We work with raw XCH_4 because the neighborhood fixed effects remove the background in a single, transparent step: $\alpha_{n(i)}$ absorbs everything common within a roughly five hundred kilometer block, including the latitudinal background, seasonal and transport structure, and any smoothly varying regional source, so that β is identified from variation in livestock density across nearby cells that share the same background. We take logs of livestock methane because its density is highly skewed, and we interpret β as a semi-elasticity in parts per billion per log unit.

We use Tier 1 livestock methane because a total head count would treat a chicken and a cow as equivalent; the emission factor weighting is the physically grounded way to collapse the six heterogeneous species into one methane-relevant quantity, and the weights come from the IPCC inventory guidelines rather than from the satellite, so the regressor is not fitted to the outcome. Section 4.1 confirms that the regression does not depend on this choice.

Identification rests on the assumption that, within a neighborhood, cells with more livestock do not systematically differ in unobserved methane sources in a way correlated with livestock. This is not an assumption of random assignment, and we do not claim a causal effect of livestock on the column. What we claim is narrower and appropriate to a measurement question: that the satellite column carries information about the spatial distribution of livestock once the neighborhood background is absorbed. We estimate Equation (1) separately by continent, because the descriptive patterns and the estimates both indicate that the relationship is heterogeneous, and a pooled coefficient would average over economically distinct regimes.

We assess discriminant validity by adding a vector of controls X_i, the log rice fraction, log fossil methane from the GFEI oil, gas, and coal inventory, and log waste methane from the EDGAR landfill and wastewater sectors, so that the specification becomes

$$y_i = \beta \log \ell_i + X_i'\eta + \alpha_{n(i)} + \varepsilon_i. \tag{2}$$

We report a battery of specification checks: a pooled regression adds the controls one at a time and varies the neighborhood block from three to ten degrees, and we re-estimate with animal units, ruminant head counts, and a species horse race. The gradient survives every variant and shows a robust and significant relationship between livestock activity and methane emissions.

3.2 Detection and Prediction Using Machine Learning Models

We then use XGBoost models to detect the non-linear relationship between livestock and satellite methane. To decompose the signal into interpretable drivers, and in particular to see how livestock compares with fossil, waste, and rice, we predict the XCH_4 from twelve features: the six livestock species, rice fraction, GFEI fossil methane, EDGAR waste methane, and three geographic terms, using gradient-boosted trees (Chen and Guestrin, 2016). Trees capture nonlinearity and interactions

that a linear model would miss.

A tree ensemble has no fixed effects, so the neighborhood demeaning that identifies Equation (1) inside the regression must here be done before estimation. For each cell i in 5° block $b(i)$ we define the block residual:

$$r_i = y_i - \bar{y}_{b(i)}, \qquad \bar{y}_b = \frac{1}{|b|} \sum_{j \in b} y_j, \tag{3}$$

where y_i is raw XCH_4, and the block mean is taken over the cells of the same block with valid retrievals in the same year. This is the within transformation computed in advance, so the background is removed before estimation rather than by fixed effects. To interpret the model results, we compute Shapley values, which allocate the model prediction across features in a way that is additive and consistent, and we rank features by mean absolute Shapley value as a measure of importance (Lundberg and Lee, 2017).[4]

4 Global Evidence on Livestock-Related Methane

4.1 The Spatial Livestock–Methane Relationship

Our first finding is that, conditional on the local neighborhood, cells with more livestock carry more methane. We first regress grid-cell methane concentration on livestock activity. We test two different methods for measuring livestock. First, we use "animal units," which is a way to weight different types of animals based on their size. For example, a cow is weighted more heavily than a sheep. Second, we use a simple "head count" of all ruminants, such as cattle and goats.

Table 1 presents the results in a single pooled regression that averages across continents using animal units, the standard body mass-based aggregation used in agricultural statistics, and the raw ruminant head count. The results in Panel A show a large and precisely estimated relationship between satellite methane and animal units. Panel B shows that a simple count of ruminants is also a strong predictor of methane, though the coefficients are somewhat lower. Even after we account for other sources of methane, including rice farming, oil and gas operations, and waste, the coefficient remains high.

The correlation does not depend on how we measure livestock activity. We then use a species horse race specification to reinforce which animals carry the signal and show why the weighting matters. Panel C in Table 1 presents the six species' head counts jointly. Cattle and buffaloes emit the most per head, and they load strongly and positively across every control set. The four ruminant species are jointly significant. The smaller species, though, are spatially collinear with the ruminants and with the confounders, so their individual coefficients are unstable and cannot be fully interpreted as emissions. Sheep even turn negative, and pigs and poultry are significant only because they proxy for dense agricultural regions.

[4] Appendix A4.1 offers more details on how we compute the Shapley values for each input feature.

Table 1. Methane concentrations and measures of livestock activity

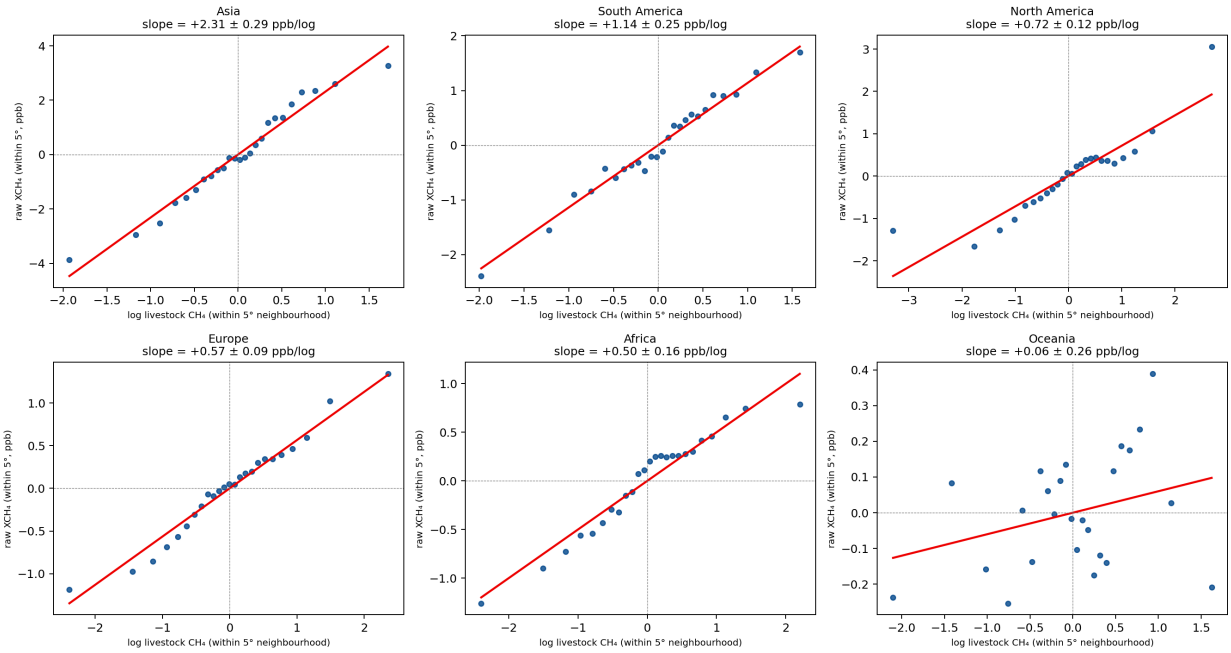
	(1)	(2)	(3)	(4)
Panel A. Log animal units (tropical livestock units)				
Animal units	0.991***	0.946***	0.975***	0.867***
	(0.085)	(0.080)	(0.084)	(0.076)
Within R^2	0.061	0.075	0.066	0.090
Panel B. Log ruminant head count				
Ruminant head count	0.762***	0.727***	0.749***	0.659***
	(0.076)	(0.073)	(0.075)	(0.070)
Within R^2	0.036	0.051	0.041	0.071
Panel C. Relationship between satellite methane and livestock species				
Cattle	0.661***	0.637***	0.656***	0.607***
	(0.091)	(0.090)	(0.091)	(0.089)
Buffaloes	0.895***	0.854***	0.892***	0.854***
	(0.243)	(0.240)	(0.241)	(0.237)
Sheep	−0.313***	−0.314***	−0.310***	−0.307***
	(0.095)	(0.094)	(0.095)	(0.093)
Goats	0.327***	0.331***	0.321***	0.299***
	(0.086)	(0.085)	(0.085)	(0.084)
Pigs	0.155**	0.133*	0.154**	0.124*
	(0.070)	(0.068)	(0.070)	(0.067)
Poultry	0.130***	0.126***	0.125***	0.109***
	(0.035)	(0.035)	(0.035)	(0.034)
Ruminants, joint p	< 0.001	< 0.001	< 0.001	< 0.001
Non-ruminants, joint p	< 0.001	< 0.001	< 0.001	< 0.001
Within R^2	0.095	0.103	0.098	0.116
Rice control	No	Yes	No	Yes
Oil/gas control	No	No	Yes	Yes
Waste control	No	No	No	Yes
Neighborhood FE	5°	5°	5°	5°
Observations	647,529	647,529	647,529	647,529

Notes: This table reports pooled OLS estimates of raw satellite methane (XCH_4) on alternative measures of livestock activity. Panel A uses FAO tropical livestock unit weights. Panel B ruminants include cattle, buffaloes, sheep, and goats. Panel C reports head counts for six livestock species jointly. All models include 5-degree by 5-degree neighborhood fixed effects and use the 2019 land sample. The control rows at the bottom apply to all panels. Standard errors (in parentheses) clustered at the neighborhood level. All regressors are transformed using $\log(1+x)$. $^{*}p < 0.1$, $^{**}p < 0.05$, $^{***}p < 0.01$. Source: AGLW, GlobalRice20, GFEI, EDGAR.

Figure 4 shows binned means of raw XCH_4 against log livestock methane by continent for 2019. The relationship is positive on five of six continents. The results show that there is a relationship between livestock activity and methane emissions, with 2.31 parts per billion per log unit of livestock methane in Asia, followed by 1.14 in South America, 0.72 in North America, 0.57 in Europe, 0.50 in Africa, and a statistically insignificant 0.06 in Oceania (Appendix Table A4 and Table A5).[5] The

[5]Our findings remain consistent across various model specifications and different methods for clustering standard

Figure 4. Satellite methane and livestock density by continent



Notes: This figure shows average satellite methane levels XCH_4 compared to the amount of livestock methane. Both variables are adjusted to account for differences between 5° by 5° neighborhoods. The dots represent average values for different groups. Data are presented for each continent using 2019 records. Source: GHAP XCH_4 and AGLW.

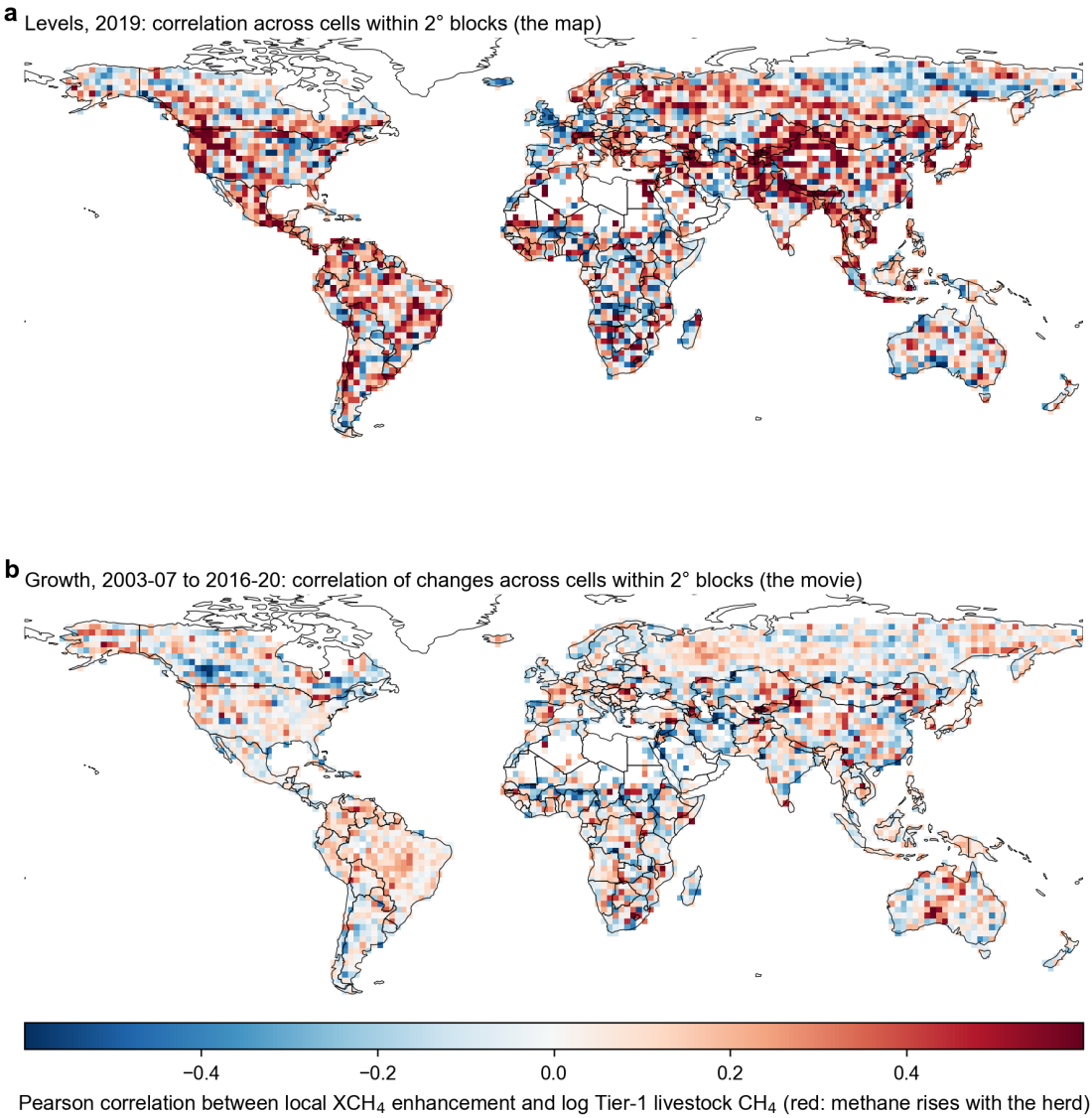
results indicate a small enhancement relative to the roughly 1,800 ppb benchmark, which is exactly what one expects from a diffuse surface source seen through a column-integrating instrument, and it is why the signal is invisible in the levels themselves and emerges only once the neighborhood fixed effects absorb the regional background.

The result is robust along two dimensions. First, it survives spatially correct inference. Raw XCH_4 is strongly spatially autocorrelated, so we compute Conley spatial standard errors in addition to neighborhood clustering, which allow errors to correlate across cells up to 500 kilometers apart. The estimation remains significant on five of six continents even under a 500-kilometer Conley kernel (Appendix Figures A5 and A7). Second, it passes a falsification test. Reshuffling livestock density within neighborhoods collapses every continental coefficient to essentially zero, which confirms that the estimate reflects the genuine cell-level co-location of livestock and methane rather than a mechanical bias of the fixed effects.

Figure 5 maps the correlation between the local methane enhancement and Tier-1 livestock methane across the cells of each 2° square, in 2019 levels in panel (a) and in 2003 to 2020 changes in panel (b). The level correlation is positive over most livestock regions, 61 percent of blocks with a median of 0.08, whereas the change correlation is centred on zero, 53 percent of blocks with a median of 0.01 and no coherent regional pattern, which is the spatial form of the paper's result that the column records where the herd is but not where it grew.

errors, as shown in Panels (b) and (c) in Appendix Figure A6.

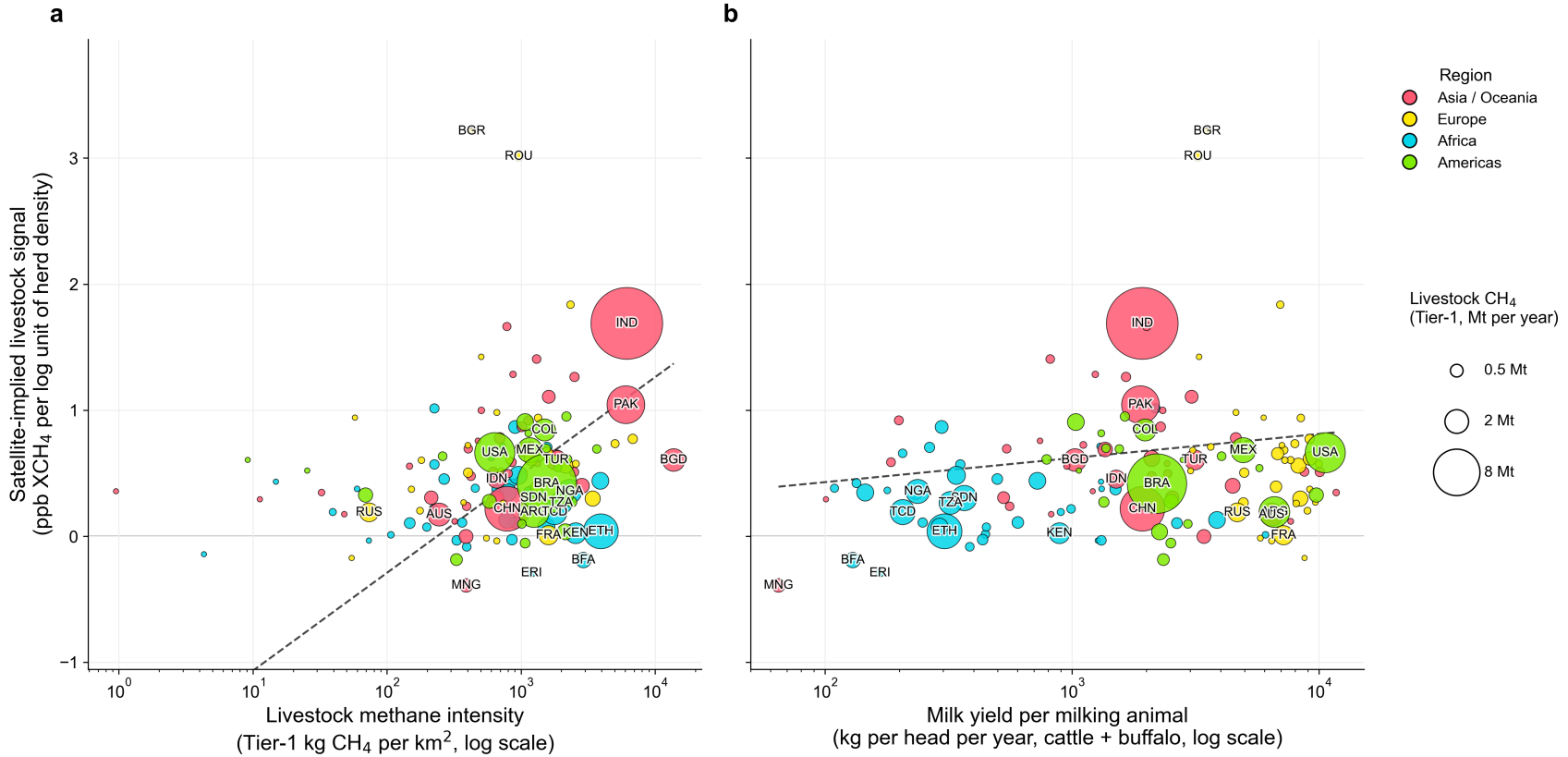
Figure 5. Local correlation between column methane and livestock



Notes: Both panels use raw GHAP XCH_4 at 0.1° and Tier-1 livestock methane from AGLW densities with IPCC Tier-1 factors, with no background filter, and each colored 2° × 2° block shows the Pearson correlation across its 0.1° cells between local methane enhancement (raw annual XCH_4 minus its 5° neighborhood mean) and livestock methane. Red marks blocks where methane is higher or rose more with more livestock, blue the opposite.

Figure 6 places each country by the strength of its satellite-implied livestock signal, the within-neighborhood gradient of raw XCH_4 on herd density estimated on that country's own cells, against livestock methane intensity in panel (a) and milk yield per milking animal in panel (b). Detectability rises with ruminant density, with India, Pakistan and Bangladesh at the top, but is unrelated to how productive the animals are: the high-yield, large-farm systems of North America and Western Europe sit no higher than the low-yield smallholder systems of South Asia and sub-Saharan Africa.

Figure 6. Where the satellite sees the livestock: density versus productivity



Notes: Each bubble is a country. The horizontal axis is Tier-1 livestock methane intensity (kg CH_4 per km^2 of land, log scale) from AGLW 2019 densities and IPCC Tier-1 factors (cattle 62, buffaloes 55, sheep 8, goats 5, pigs 1.5, poultry 0.02 kg per head per year). The vertical axis is the satellite-implied livestock signal, the coefficient on log(1 + Tier-1 CH_4 density) from a country-by-country regression of GHAP XCH_4 (2019, 0.1°) on that density with 2° neighborhood fixed effects and log fossil and waste controls, in ppb per log unit.

4.2 Attribution of the Livestock Methane Signal

A positive coefficient is necessary but not sufficient for the satellite to measure livestock specifically, because livestock co-locates with other methane sources, biogenic and fossil alike. We address this in two ways. First, within the regression framework, we add three direct controls: rice fraction, oil, gas, and coal methane taken cell by cell from the GFEI fossil fuel inventory (Scarpelli et al., 2022), and landfill and wastewater methane from the EDGAR sectoral grids. These are the actual confounding sources mapped to the grid, not a residual. They attenuate the coefficient only slightly and do not remove it (Appendix Table A4). The within-neighborhood livestock signal is not fossil methane, waste methane, or rice in disguise.

Second, and more revealing, the machine learning attribution decomposes the local residual into interpretable pieces. Panel (a) of Figure 7 ranks the features by mean absolute Shapley value using an XGBoost model, with the target the fixed-effect residual, raw XCH_4 minus its 5° block mean. The three geographic terms are the largest features, at 0.61, 0.61, and 0.53 parts per billion for latitude, longitude, and absolute latitude, more than twice the largest source feature. Subtracting the average value for each 5° block removes differences between regions, but it does not account for variation within a single block. Factors such as wetlands, terrain, and satellite sensitivity vary within these areas. Since our datasets do not include these factors, the model uses geographic coordinates to represent them.

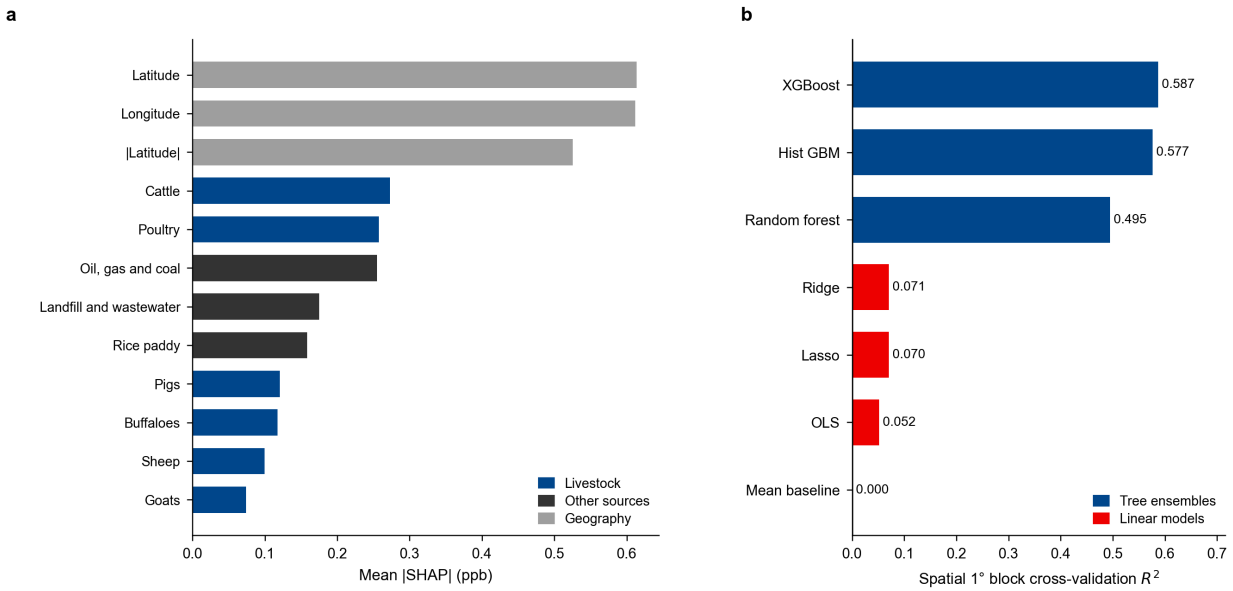
Livestock, fossil fuels, waste, and rice all have similar effects on local methane levels. For this reason, we cannot link satellite methane to livestock without accounting for these other sources. Our empirical design does exactly this. We use neighborhood fixed effects to remove the influence of large oil and gas fields and regional patterns. We also use specific controls for fossil fuels, waste, and rice to account for other sources found near livestock.

We report the predictive performance of each model in Figure 7, Panel B, and Appendix Table A7. The most accurate model, the gradient-boosted trees, achieves an R^2 of 0.59 and a root mean squared error of 2.54 parts per billion. Predicting the sample mean everywhere gives 3.95, so the best model improves on a no-skill baseline by 36 percent. Results for the mean absolute error are similar, with an error of 1.81 for the gradient-boosted trees compared to 2.87 for the baseline. The linear models perform poorly, with R^2 values between 0.05 and 0.07, indicating that the relationships in the data are nonlinear.

4.3 Atmospheric Placebo Tests

We perform an additional test that focuses on other gases in the air. Direct controls handle only the sources we can name. The broader concern is unobserved correlates of livestock location, such as infrastructure or emission-trapping geography. If unobserved factors of this kind drove the results, similar patterns would appear in pollutants that livestock do not produce. To test this, we repeat our main analysis but replace methane with other pollutants that livestock do not produce. The sample, design, and fixed effects are unchanged; outcomes are standardized because the gases are measured in different units.

Figure 7. What the model learns on, and how well it does



Notes: Both panels describe the results from the same model. The variable we predict is the difference between raw satellite methane and the average for each five-degree block. The model is estimated using 2019 data for areas with livestock and tested on separate one-degree blocks. Panel A shows the importance of each factor based on its average Shapley value. Panel B compares the R^2 of different models against a simple average. Sources: GHAP, AGLW, GlobalRice20, GFEI, and EDGAR.

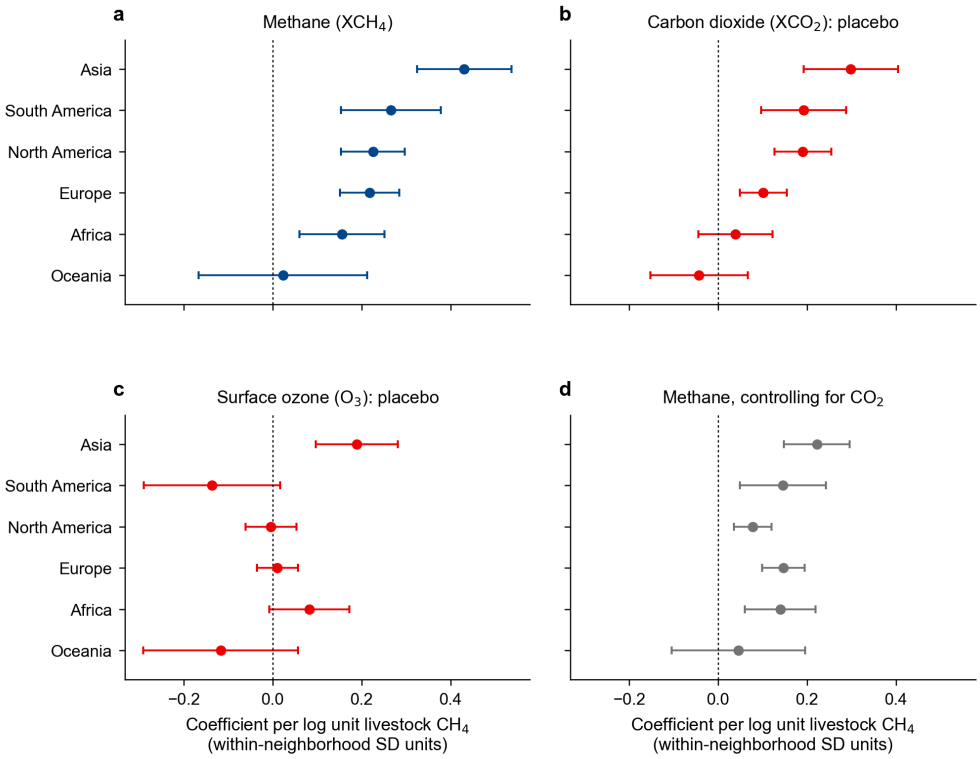
Figure 8 reports two results. First, surface ozone acts as a proper control. Its overall effect is small, only 0.04 standard deviations compared to 0.22 for methane, and it is not statistically significant in North America or Europe. In Asia, we find a positive result, which is likely due to crop burning or local chemistry common in intensive farming areas. Second, carbon dioxide provides a more difficult test, and the results are less clear. Its effect is positive and significant across four continents and is about two-thirds the size of the methane effect. This indicates that areas with many animals also have higher carbon dioxide levels. This could be due to other human activities, crop farming, or the way local geography traps multiple gases.[6]

We aim to remove the factors that influence both methane and carbon dioxide. By adding carbon dioxide levels as a control, we can account for external factors that increase both gases and isolate the variation that is specific to methane. The methane coefficient decreases but remains statistically significant in all regions where it was originally present. Specifically, the overall coefficient falls from 0.79 to 0.47 parts per billion. In Asia, it drops from 2.31 to 1.19, while in Africa, it remains nearly unchanged, falling from 0.50 to 0.45. This is because carbon dioxide levels in Africa were already near zero, so accounting for them has little effect. In Oceania, the results remain close to zero across all models.

Overall, about 60 percent of the methane coefficient remains after controlling for carbon dioxide (0.47 of 0.79 parts per billion). This share cannot be attributed to human activity or terrain that

[6]Appendix Table A6 provides the detailed results for each continent.

Figure 8. The livestock coefficient is specific to methane



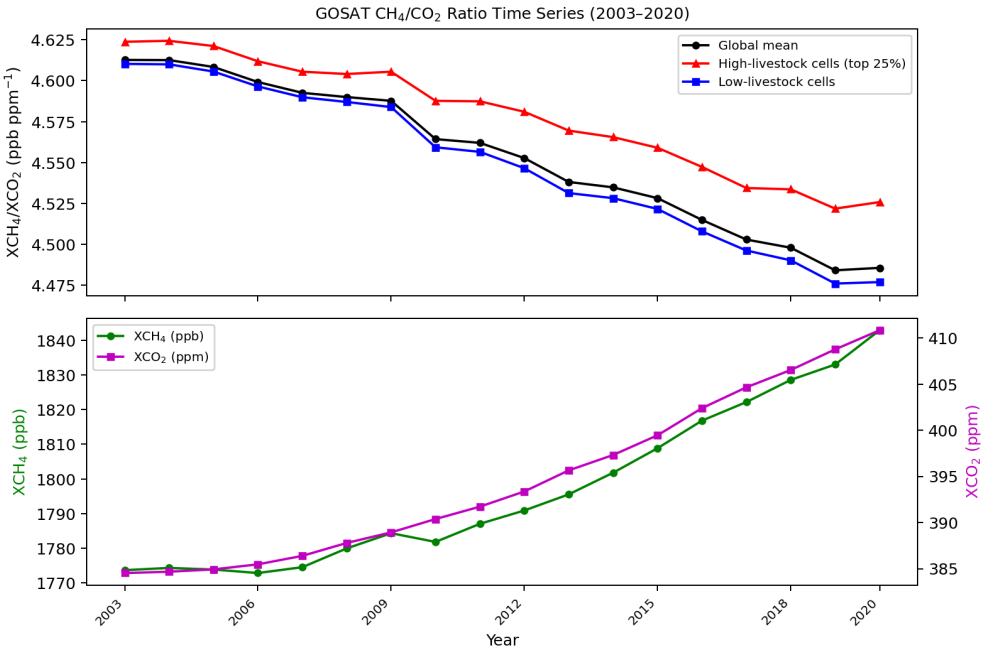
Notes: Coefficients on log Tier-1 livestock methane by continent, in standard deviations of each outcome gas, with 95 percent confidence intervals. Panel (a): column methane. Panels (b) and (c): column carbon dioxide and surface ozone, placebo pollutants that livestock do not emit. Panel (d): methane after controlling for XCO_2, which absorbs factors common to both columns. All regressions use the 2019 land sample with 5° neighborhood fixed effects. Source: GHAP XCH_4, XCO_2, and O_3; AGLW.

raise both gases, because carbon dioxide from the same instrument absorbs those common factors. The methane-specific share ranges from about one-third in North America, where the two gases move together most closely, to nearly nine-tenths in Africa. Because this test does not require identifying the confounder, it covers sources our direct controls miss, but only those that also raise carbon dioxide.

Our results suggest that livestock methane comes from biological sources as opposed to fossil fuels. Further physical evidence supports this conclusion. Fossil fuel combustion releases CO_2 alongside methane; biogenic sources emit methane with little co-located CO_2. The methane-to-carbon dioxide ratio should therefore be higher where biogenic sources dominate. When we group locations by their primary source of emissions, we find that the average ratio is highest in rice-growing areas (4.587) and livestock regions (4.557). The lowest ratio occurs in oil and gas regions (4.553), as shown in Appendix Figure A8. This ratio consistently increases in areas with higher livestock density or more rice farming.

This pattern also changes over time. Figure 9 traces the GOSAT methane to carbon dioxide ratio from 2003 to 2020. The global ratio falls steadily, from about 4.61 to 4.49 parts per billion per

Figure 9. The biogenic fingerprint over time



Notes: The top panel displays the ratio of methane to carbon dioxide from 2003 to 2020. The black line represents the global average, the red line represents the 25 percent of areas with the most livestock, and the blue line represents areas with very few animals. The bottom panel shows the individual levels of methane and carbon dioxide used to calculate these ratios. The global ratio falls as carbon dioxide rises faster than methane, but the excess of high livestock over low livestock cells widens from 0.014 to 0.049 ppb ppm^{-1}. Source: GHAP XCH_4 and XCO_2.

part per million, because column carbon dioxide rose faster than column methane over the period. Against this general decline, the gap between the highest- and lowest-livestock cells widened from 0.014 to 0.049 ppb ppm^{-1}, a difference that is statistically significant: even as the global ratio falls, high-livestock regions separate further from the rest. The same widening appears region by region (Appendix Figure A9). The ratio declined the least in South Asia and Sub-Saharan Africa, which are regions where livestock are common and where herds grew the fastest during this period. These findings are consistent with the idea that increasing livestock activity is leaving a larger biological mark on the atmosphere.[7]

The absolute gaps across source regimes are small, as they must be: the column integrates the whole atmosphere, and surface emissions are a small share of it. The ordering, however, is consistent, with biogenic regimes above fossil ones, so we read the ratio as corroborating a biogenic origin for the methane over livestock and rice regions.

[7]This analysis compares broad groups of cells over eighteen years; it does not imply that year-to-year changes are detectable in small areas. Normalizing methane by carbon dioxide from the same instrument removes transport and retrieval noise common to both columns. One further caveat: the series spans GHAP's 2009–2010 transition from SCIAMACHY to GOSAT retrievals, so ratio levels are not directly comparable across that break. The widening gap between high- and low-livestock cells is similar when the sample is restricted to the GOSAT years, 2010–2020.

5 When Satellite Methane Reveals Livestock Activity

In this section, we discuss what the satellite can detect and why. We use data from the United States for validation for several reasons. The United States has the most detailed livestock records in the world, through the Census of Agriculture and USDA surveys, and is therefore the natural benchmark. We first confirm that our gridded livestock data match those records, then repeat the earlier tests from the national level down to the county.

5.1 County-Level Validation in the United States

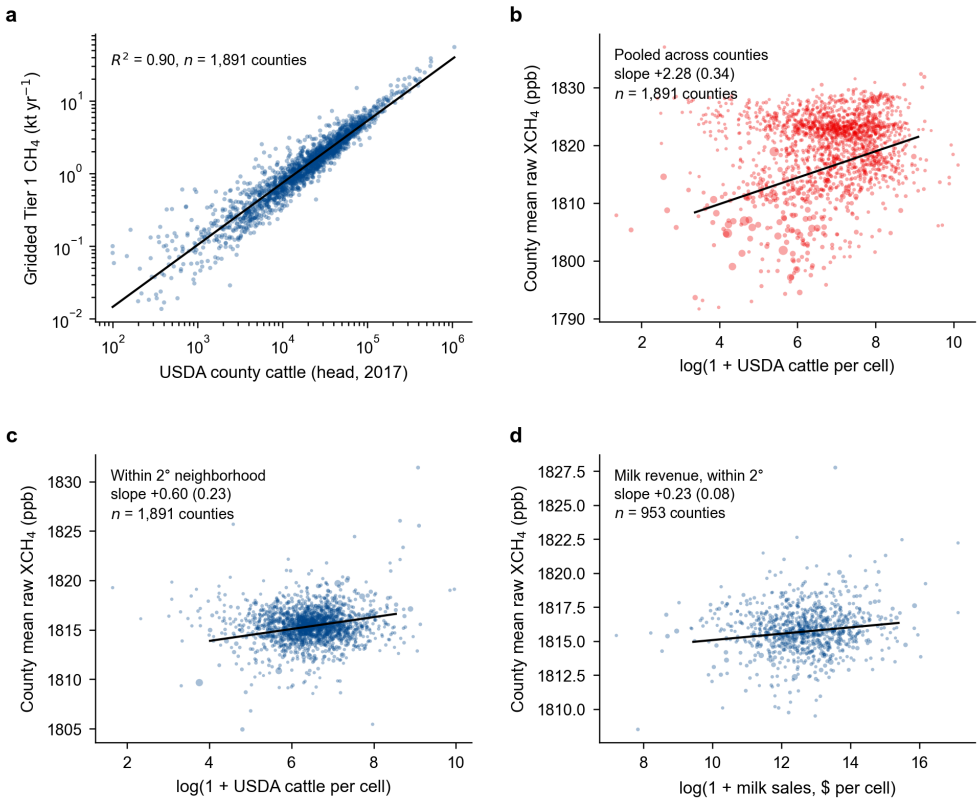
We first confirm that our gridded livestock product is reliable against that benchmark. We aggregate to counties and reproduce the county census with an R^2 of 0.90 across 1,891 counties (Figure 10a). It is not a test of the satellite, since the gridded product is built from census data. Panels (b) and (c) of Figure 10 show the correlation between cattle and methane emissions at the county level. Regressed on log county cattle across the 50,547 grid cells, the raw column now rises with the herd, at 2.53 parts per billion per log unit, and adding the fossil, waste, and rice controls leaves 2.08. Imposing the 2° neighborhood fixed effects, so that cells are compared only with nearby cells, gives 0.52, and adding the controls on top gives 0.53. Panel (d) of Figure 10 replaces the head count with the value of milk sold, and within the same 2° neighborhoods the column rises by 0.27 parts per billion per log dollar, and by 0.26 once the competing sources are controlled. Appendix Table A9 shows that these findings remain strong even after we add more controls.

5.2 Concentrated Dairy and Dispersed Beef Production

United States cattle are mostly beef, raised on dispersed range where enteric methane is emitted at low density over vast areas, whereas dairy cattle are concentrated in large operations whose manure lagoons release methane from a small point source. The two should therefore differ sharply in detectability even though both are "cattle." We test this by putting the USDA county census of dairy and beef cattle onto the 0.1° grid and regressing raw satellite XCH_4 on each, with neighborhood fixed effects absorbing the background exactly as in the global specification. Because a single country spans few 5° blocks, we use a 2° neighborhood as the main window and report 1° and 5° alongside it.

Satellite methane tracks dairy cattle, not beef cattle. Table 2 shows our findings. The main result comes from comparing the separate results for each cattle type with the results when they are tested together. When tested one at a time, both types of cattle show a positive relationship with the satellite data. In the 2° specification, the dairy coefficient is 0.43, and the beef coefficient is 0.52. However, when we test them together, the results change. The dairy coefficient remains strong at 0.36, but the beef coefficient falls to 0.11 and is no longer statistically significant. We see the same pattern in the 1° specification. In that case, the dairy coefficient is 0.21, while the beef coefficient is nearly zero at 0.02.

Figure 10. At county resolution, the satellite tracks the herd



Notes: Panel A shows estimated livestock methane compared to official cattle counts from the United States Department of Agriculture (USDA). Panel B shows satellite methane readings compared to the number of cattle per area across the entire country. Panel C repeats this comparison after accounting for local differences within two-degree neighborhoods. Panel D shows satellite methane compared to the value of milk sales in dollars. Sources: GHAP and the USDA Census of Agriculture.

These findings suggest that beef cattle only seem to matter because beef counties are often located near dairy counties. Once we account for both types at once, the satellite data follows dairy cattle and not beef cattle. Appendix Figure A15 illustrates this point. When we control for the presence of one cattle type, the relationship for dairy cattle increases while the relationship for beef cattle stays flat. In the largest 5° window, dairy cattle still show a larger effect than beef cattle.

Measurement of local farm economy and livestock activity. The last step relates our results to economic variables. Using data from the Census of Agriculture, we replace the number of dairy cattle with the total value of milk sales at the county level and repeat our estimation. Appendix Table A8 presents the results. Among the 953 counties that report milk sales, we find that satellite methane levels increase alongside the value of milk sold. Specifically, methane levels rise by 0.27 parts per billion for every one-log-dollar increase in milk sales. This result is statistically significant at the 1 percent level. These findings show that the satellite signal carries information

Table 2. Satellite methane tracks dairy cattle, not beef cattle

	(1) Dairy only	(2) Beef only	(3) Both
Panel A. 1° neighborhood (811 blocks)			
Log dairy cattle	0.229*** (0.045)		0.214*** (0.060)
Log beef cattle		0.266*** (0.060)	0.025 (0.073)
Panel B. 2° neighborhood (240 blocks), main			
Log dairy cattle	0.427*** (0.097)		0.364*** (0.116)
Log beef cattle		0.525*** (0.137)	0.112 (0.150)
Panel C. 5° neighborhood (46 blocks)			
Log dairy cattle	0.485* (0.276)		0.383 (0.412)
Log beef cattle		0.672** (0.310)	0.207 (0.406)

Notes: Raw satellite XCH_4 (2010–2020 mean) on log county cattle per 0.1° cell, with neighborhood fixed effects and standard errors clustered by neighborhood. Columns (1) and (2) enter each cattle type alone; column (3) enters both. Each panel varies the width of the neighborhood comparison window. $n = 50{,}547$ cells throughout. Standard errors in parentheses; $^{*}p < 0.1$, $^{**}p < 0.05$, $^{***}p < 0.01$.

about farm revenue as well as the number of livestock.

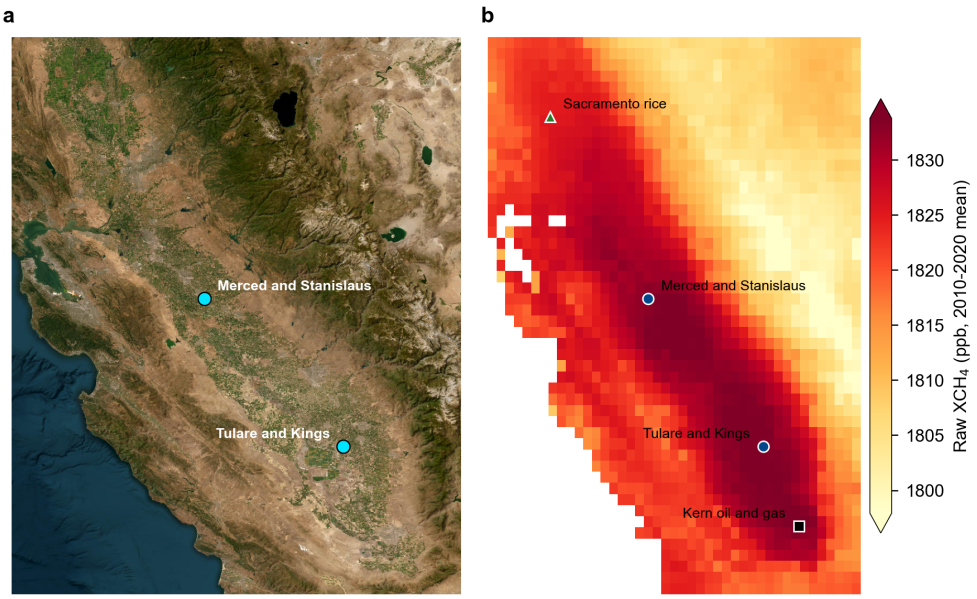
We have two interpretations of these findings. First, milk revenue and the number of dairy cows are nearly collinear. Revenue is calculated by multiplying the number of cows by the amount of milk they produce and the price of that milk. When we include both revenue and the number of cows in the same model, the number of cows accounts for almost all of the effect. This suggests that the satellite primarily detects the animals themselves, while the monetary revenue is simply another way of measuring those same animals.

Second, this part of our analysis only includes counties that report milk sales, which accounts for about half of our original sample. Therefore, the results for beef cattle in this specific group are not directly comparable to our earlier findings for the full country. Overall, this exercise shows that the satellite signal matches official records.

The case of California's dairy farms. We examine dairy farms in California to provide further evidence for our findings. California's Central Valley has the highest concentration of dairy farms in the country and is a methane hotspot. Figure 11 compares images of this area with the raw satellite data. Within the valley, we measured methane levels across four subregions. In the dairy centers of *Tulare and Kings*, methane levels average 1,833 ppb. The levels in *Merced and Stanislaus* average 1,832 parts per billion. In comparison, the *Kern oil and gas* fields average 1,831 parts per billion, while the *Sacramento rice belt* averages 1,825 parts per billion. The overall average for the entire region is 1,819 parts per billion.

We approach this comparison with caution. Methane levels are high throughout the entire valley because the geography traps emissions. As a result, the areas with many dairy farms represent the highest point of a large methane cloud that covers the valley, rather than a single, isolated source. The difference in methane levels between dairy areas and oil and gas fields is small, at only one

Figure 11. The largest dairy cluster sits on the valley methane maximum



Notes: (a) Esri World Imagery over California's Central Valley with the two dairy cores marked. (b) Raw GHAP XCH_4 over the same window, 2010 to 2020 mean, in absolute parts per billion with no background removed, with the dairy cores, the Kern oil and gas fields, and the Sacramento rice belt marked. The whole valley is elevated because its topography traps emissions; the dairy cores are its maximum, and the margin over the co-located fossil fields is one to two parts per billion. Source: Esri World Imagery and GHAP.

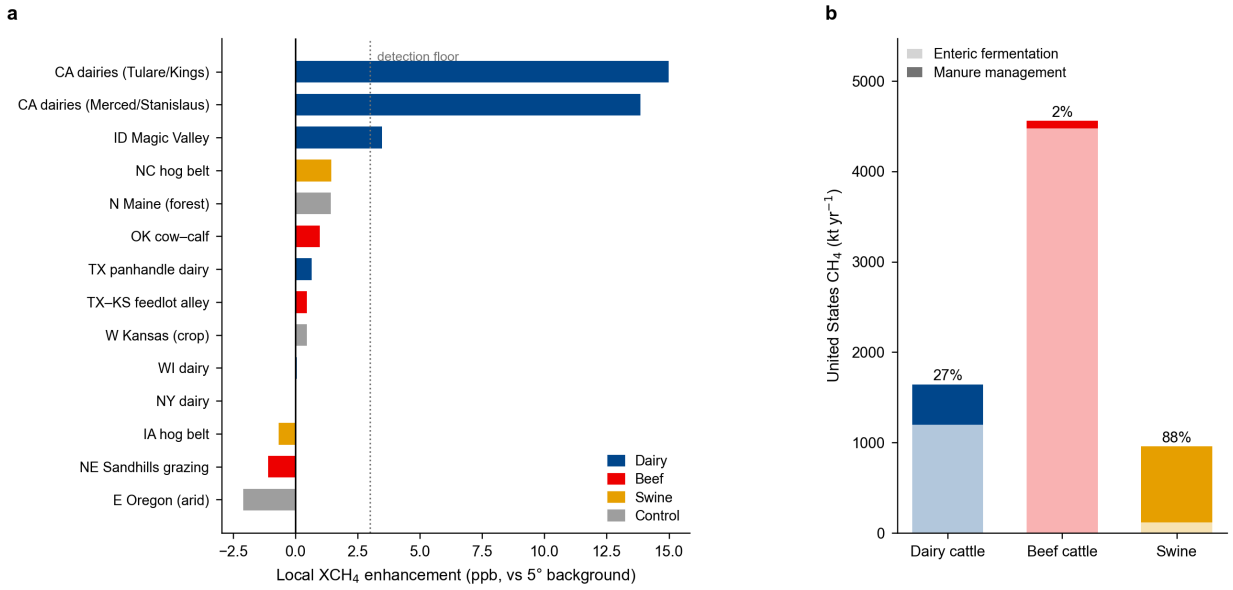
to two parts per billion. This difference is minor compared to the 14 ppb gap between the dairy centers and the regional average.

Our data show that the dairy centers have the highest methane levels, while the rice-growing areas have the lowest of the four counties (Tulare, Kings, Merced, Stanislaus). This finding aligns with previous studies that identify Central Valley dairy farms as a major regional source of methane (Duren et al., 2019). Calculating the exact share of emissions from dairy versus oil and gas would require more advanced measurements, which we do not attempt here.

Satellite methane instruments fall into two families. Column instruments, like the one behind GHAP, average the full atmosphere over cells roughly 11 kilometers wide and resolve enhancements of a few parts per billion. Plume imagers instead resolve meter-scale scenes and detect individual plumes when a source is strong enough, which is how ultra-emitting oil and gas leaks are found (Lauvaux et al., 2022) and individual facilities monitored (Varon et al., 2021). The two families share a blind spot: dispersed sources. A plume imager can see a dairy's waste lagoon, where manure methane concentrates into a point source, but not beef cattle grazing across a field, whose enteric emissions are released animal by animal and never cohere into a plume; a column instrument needs the same spatial concentration to lift an 11-kilometer average. That shared geometry is what the dairy–beef contrast in Table 2 measures, and independent aircraft campaigns over California reach the same conclusion (Duren et al., 2019).

These instruments corroborate our results but cannot substitute for global, annual coverage.

Figure 12. What the satellite can detect, and why



Notes: (a) Local XCH_4 over ten United States livestock regions, ordered by magnitude, against the surrounding 5° background, GHAP 2010–2020. The dotted line marks the approximate GOSAT detection floor. Single-blind controlled releases place the floor of current point-source instruments at roughly 50–200 kg hr^{-1} (Reuland et al., 2026); the column-average floor shown here is coarser because GHAP integrates over an 11-kilometer cell. Only the California Central Valley dairy complex clears the floor decisively, at 8.1 ppb, with Idaho's Magic Valley marginal at 3.5, while every beef region and the smaller hog belts sit at or below it. (b) United States livestock methane by emission channel, FAOSTAT Tier 1, 2020, with the manure share printed above each bar; the solid segment is manure management and the pale segment enteric fermentation. Panel (b) supplies the mechanism. Manure management is a concentrated lagoon source and is 27 percent of dairy and 88 percent of swine methane but only 2 percent of beef, which is dispersed enteric fermentation. Detectability therefore needs both a high manure share and enough scale, which in the United States essentially one region has. Colors denote the production system. Source: GHAP and FAOSTAT.

The division of labor is the reverse: column measures locate livestock-dominated airsheds; plume imagers attribute emissions to individual farms. Our method measures methane in areas where livestock is the main source, while specific imagers can link emissions to particular farms. This second type of measurement is exactly what United States law currently prevents from being collected on the ground.

Appendix Figure A16 maps both gases, with the largest dairy counties outlined in red. The country's largest dairy concentration sits on the state methane maximum in the raw data, before any background removal. The dairy counties of the southern Central Valley read about 1,830 ppb against a state average of 1,809. The carbon dioxide map is less informative on its own. The valley's topography traps every gas released inside it, and the floor also holds cities, traffic, and crop agriculture, so the maps alone cannot separate the sources. Appendix Table A6 shows the dairy–methane relationship remains strong when controlling for carbon dioxide.

Smaller and more dispersed operations are not detectable at GHAP resolution. The North Carolina and Iowa hog belts and the Texas and Kansas feedlot alley are indistinguishable from

rural controls (Figure 12a). The mechanism that separates the detectable from the undetectable is the concentrated manure channel. FAOSTAT shows that manure management, the anaerobic lagoon source, is 27 percent of dairy methane and 88 percent of swine methane but only 2 percent of beef methane, which is mostly enteric and produced by dispersed grazing animals (Figure 12b). Dairies and large hog operations concentrate methane in lagoons, and the very largest such clusters clear the detection floor, while beef does not concentrate methane at all. Detectability therefore requires both a high manure share and sufficient scale, and only the Central Valley meets both at this resolution.

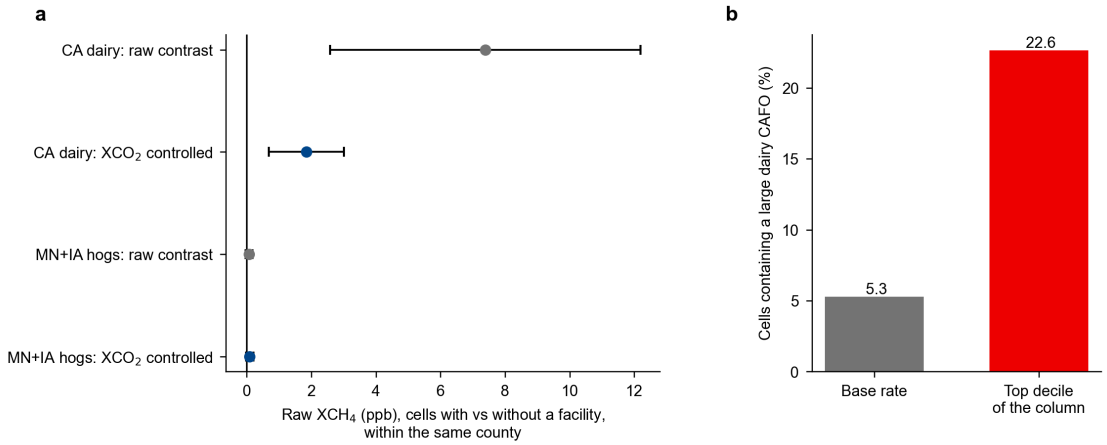
This finding has a policy edge because the United States does not measure facility-level livestock methane. The greenhouse gas reporting program contains no manure management data, owing to a long-standing appropriations rider that bars its collection, so federal livestock methane at the facility level is modeled rather than measured. The satellite already detects the largest clusters, and finer instruments will lower the threshold, so remote sensing could begin to fill a genuine measurement gap. In companion work, Beatty et al. (2026) show what filling it looks like in practice: using facility-scale airborne retrievals over California dairies, they evaluate a manure-management subsidy against realized emissions—program evaluation conducted inside the detection envelope this section maps.

5.3 Facility-Level Validation and the Detection Envelope

The facility records allow a sharper version of this test, because the mechanism is a claim about facilities, not about counties. If the spatial concentration of livestock is what makes methane visible, then within the same county, holding the census herd fixed, the grid cells that actually host a dairy operation should read higher than the county's other cells. We run exactly that comparison in California, where the permit records cover about two-thirds of the census dairy herd. One adjustment is essential. California counties straddle the valley floor and the Sierra, and a column mixing ratio is mechanically depressed over high terrain, so a naive within-county contrast of 7.4 parts per billion overstates the facility signal badly. Raw XCO_2 from the same instrument shares that column geometry but not the livestock source, and controlling for it cuts the contrast to 1.8 parts per billion with a t statistic of 3.1, with a dose response of 0.23 parts per billion per log head of recorded facility capacity. Three-quarters of the naive contrast was terrain; what survives is a facility-level methane signal, measured rather than inferred (Figure 13a).

The same design in the hog belt returns nothing, which is what the detection envelope predicts at facility level. Minnesota and Iowa hold the densest coverage with more than a thousand treated cells, and hog manure is the most lagoon-intensive channel of all, yet cells hosting hog operations read only 0.09 parts per billion above their county neighbors. Manure share alone is not sufficient. The operations must also be large enough, and midwestern hog sites are an order of magnitude below the California dairies in animal mass per cell. Finally, the facility file lets us score the detector of Section 5.4 against real operations rather than a census proxy. The top decile of the within neighborhood column in California contains a large dairy operation in 22.6 percent of cells

Figure 13. The spatial concentration mechanism, tested at the facility level



Notes: (a) Within-county contrast in raw XCH_4 between cells that do and do not host a confined animal feeding operation, from state permit records, 2010 to 2020 means; bars are 95 percent confidence intervals, clustered by 2° neighborhood. Grey estimates are the naive contrast; blue estimates control for raw XCO_2 from the same instrument, which absorbs the mechanical depression of any column mixing ratio over high terrain. (b) Share of California cells containing a large dairy operation, 700 or more head, among all cells and among the top decile of the within neighborhood methane column. The California dairy signal survives the terrain control at 1.8 ppb; the Minnesota and Iowa hog signal is absent in both versions, because those operations are an order of magnitude smaller in animal mass per cell. Facility coverage is validated against the USDA herd state by state, and unrecorded facilities bias the contrasts toward zero. Source: state permit records compilation, GHAP, USDA NASS.

against a 5.3 percent base rate, a lift of 4.3 (Figure 13b).

The facility data also lets us replicate, and then test, the structure of the new asset-level inventories. Climate TRACE estimates each operation's methane bottom up, as estimated head times an emission factor (Davitt et al., 2026). We rebuild that object on the permit records with factors implied by the accounting used throughout this paper: FAOSTAT's United States totals for 2020 divided by the NASS herd give 176 kilograms per dairy cow, 51 per beef animal, and 12 per hog, and facility methane is head times factor. Regressed on the column within counties, with the XCO_2 control, California cells gain 0.15 parts per billion per log kilogram of bottom-up facility methane (Table 3, Panel A). Even the hog belt, a null in the presence test, shows a faint dose response in emissions units, 0.014 parts per billion per log kilogram, two orders of magnitude below California's. The detection envelope is a continuum in source strength, not a wall, and the atmosphere ranks the two regions in the same order as the inventory.

Comparing the two inventories teaches something neither shows alone. In animal numbers, they roughly agree where coverage is best: the permit records place 733 thousand head in the Tulare and Kings core against 588 thousand gridded census cattle, a ratio of 1.25 consistent with permits recording capacity rather than standing herds. In methane, they diverge by up to a factor of 3.4, and the gap is almost exactly the ratio of the dairy factor to the blended cattle factor, 176 against 62. What the asset inventory adds to a census grid is therefore not mainly location but *typing*. Knowing that the animals in a cell are dairy cows nearly triples the methane assigned to it, and

Table 3. Replicating the asset inventory and testing it against the atmosphere

Panel A: ppb of raw XCH_4 per log kilogram of facility methane

	California (dairy)		Minnesota + Iowa (hogs)	
	(1)	(2)	(3)	(4)
Log facility CH_4	0.574***	0.148***	0.014**	0.014**
	(0.176)	(0.047)	(0.007)	(0.006)
XCO_2 control	No	Yes	No	Yes
Cells	2,960	2,960	3,094	3,094
Cells with facilities	201	201	1,792	1,792

Panel B: the two inventories inside the California dairy cores

	Animals (thousand head)		Methane (kt yr^{-1})	
	Facilities	Gridded census	Facilities	Gridded census
Tulare/Kings	733	588	122.9	36.7
Merced/Stanislaus	385	736	64.3	46.0

Note: Panel A, raw XCH_4 on log facility methane, where facility methane is reported head times the implied United States emission factor (dairy 176, beef 51, hogs 12 kilograms per head per year, from FAOSTAT 2020 totals over the NASS herd). In Panel B, the animal comparison and the methane comparison disagree by construction, and the wedge is the point. The facility layer types its animals, so the dairy factor of 176 applies; the gridded census layer knows only "cattle" and applies the blended 62. The methane ratio is close to the head ratio times 176/62 in both cores (Tulare/Kings $1.25 \times 2.84 \approx 3.4$; Merced/Stanislaus $0.52 \times 2.84 \approx 1.5$). Facility head counts are permitted capacities and so bound the standing herd from above. Facility records cover about two-thirds of the California census dairy herd. $^{**}p < 0.05$, $^{***}p < 0.01$. Source: Climate TRACE reported facility layer (Davitt et al., 2026), FAOSTAT, USDA NASS, AGLW, GHAP.

the satellite sides with the typed version, since these cores are where the observed column peaks.

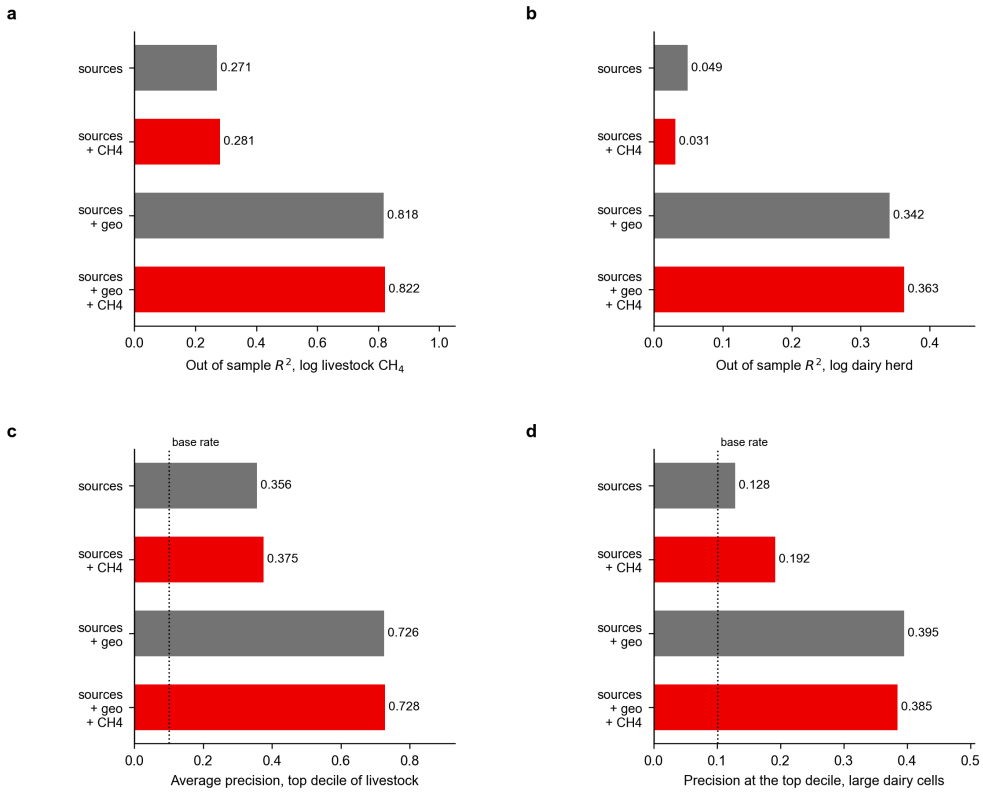
5.4 Incremental Information in Satellite Methane

The previous sections examined how livestock numbers influence methane levels. However, a statistical problem often is the opposite, which is using satellite data to estimate the size of a herd that has not yet been counted. We therefore reverse our analysis to predict livestock activity from methane levels. We focus on whether satellite data provide any new information beyond what is already available in existing records.

Our study compares a model that includes satellite data with an identical model that excludes it. The difference between the two represents the specific value added by the satellite. We test this against two benchmarks. The first benchmark includes existing data on other methane sources, such as fossil fuels, waste, and rice farming. The second benchmark adds the specific geographic location of each area. This is a more difficult test because livestock farms are often clustered together, meaning location alone is a strong predictor of where livestock are.

To ensure our results are reliable, we test our models on new areas that were not used during the initial training. We use 10-degree blocks globally and five-degree blocks in the United States. This prevents the model from appearing more accurate simply because neighboring areas are similar. We perform two tasks: predicting the total number of livestock and identifying the top 10 percent

Figure 14. The column detects large operations better than it predicts herd size



Notes: Out-of-sample performance on held-out spatial blocks, ten degrees globally and five degrees in the United States. Grey bars withhold column methane, red bars add it, so each adjacent pair is the increment attributable to the satellite. (a) Predicting log livestock methane, global 2019 cross section of 647,529 livestock cells. (b) Predicting the log dairy herd across 50,547 United States county cells, 2017. (c) Flagging the top decile of livestock density globally, average precision. (d) Flagging the top decile of dairy density in United States counties, precision at an operating point that flags as many cells as are truly positive. Source: GHAP, GFEI, EDGAR v2025, GlobalRice20, AGLW, USDA NASS.

of highest-density areas. This second task helps locate large-scale farming operations. Table 4 and Figure 14 present these results. In the figure, each pair of bars shows the improvement in accuracy gained by adding satellite information.

The results for predicting the exact size of a herd are poor, and we report them as such. Globally, adding satellite methane data to existing records only slightly improves the accuracy of our model. In contrast, simply knowing the geographic location of an area improves the accuracy significantly. For example, knowing where an area is located contributes about 0.55 to the model's accuracy in R^2 while knowing its methane levels contributes only 0.004. In United States counties, the pattern is the same. The satellite data do not provide a reliable way to estimate the size of a herd.

Identifying the largest operations is a more successful task, and the difference between these two results is important. The task is to flag the top decile of United States cells by dairy density, so a random guess succeeds 10 percent of the time. A model using only existing records flags a true top-decile cell 12.8 percent of the time; adding satellite methane raises this hit rate to 19.2

Table 4. What the column adds, on top of the inventories and on top of geography

Features	Prediction (R^2)		Detection	
	Global	US dairy	Global avg. precision	US dairy precision (lift)
Inventories only	0.271	0.049	0.356	0.128 (1.28×)
+ column methane	0.281	0.031	0.375	0.192 (1.91×)
Inventories + geography	0.818	0.342	0.726	0.395 (3.93×)
+ column methane	0.822	0.363	0.728	0.385 (3.82×)

Note: $n = 647{,}529$ global cells and 50,547 United States county cells. Inventories are GFEI fossil methane, EDGAR waste, and rice paddy fraction; geography is latitude, longitude, and absolute latitude. Column methane enters as raw XCH_4 net of its neighborhood mean, the quantity the gradient regression identifies. The single row where the satellite clearly earns its place is the United States detection task without geography, where it raises the hit rate by half. Source: GHAP, GFEI, EDGAR v2025, GlobalRice20, AGLW, USDA NASS.

percent, an improvement of one half. The global version of the task behaves the same way: the column improves the ranking of the most livestock-intensive areas even though it barely improves continuous prediction, because the largest concentrations release enough methane to stand out against the local background (Figure 14, Panels C and D).

However, geographic location remains the best predictor. A model that only knows where an area is located identifies large dairy farms with 39.5 percent precision. This is twice as accurate as the results from the satellite data alone. Therefore, satellites are not particularly useful for locating herds in countries where farming locations are already well-known and stable. Instead, the value of satellite data is in regions where geographic records are missing, outdated, or disputed. They are also useful for verifying whether reported emissions match the actual atmosphere.

This tool works outside the United States. We use a global database from Climate TRACE to verify our results. This database identifies more than 287,000 cattle farms using images and permits, rather than methane. We checked whether the areas with the highest methane levels actually contain large farms, defined as those with at least 700 dairy cows or 1,000 beef cattle. This provides a separate way to test our tool in every country covered by the database.

Eight countries had enough data to be included in this test, and Appendix Figure A17 shows the results. In China, the cells with the top 10 percent of methane readings contain a large operation 17.4 percent of the time, against a base rate of 6.7 percent, 2.6 times chance. In India the rate reaches 35.9 percent, about 1.7 times India's base rate, which is high because large operations are common there. The United States has a success rate 1.6 times better than chance. This is lower than our result of 4.3 times for California because the national data include many beef cattle, which the satellite cannot easily detect.

The satellite does no better than chance in Australia, where herds are dispersed across arid rangeland, and falls below chance in Brazil, where Amazon wetlands dominate local methane. Russia also shows a high rate, but we do not rely on it because its facility records are less complete. The satellite therefore finds large operations where livestock dominate local methane, including

China and India, whose herds are among the least well recorded. It fails where wetlands or dispersed grazing set the local methane level.

6 Discussion

6.1 Interpreting Satellite Methane as a Livestock Measure

Satellite methane carries a livestock-related spatial signal, but reading that signal requires separating livestock emissions from background variation and from competing sources. The livestock contribution must be large relative to the local methane background. This explains why the relationship is strong in some regions, such as Asia, and positive across U.S. counties. Attribution also requires controlling directly for fossil fuels, waste, and rice cultivation, which can be spatially correlated with livestock activity.

Emissions also differ sharply by species and production system. Ruminants account for 120.6 of the 122.6 megatons of Tier 1 livestock methane in our accounting (98.4 percent), while non-ruminants contribute only 2.0 megatons (Appendix Table A1). Among ruminants, concentrated dairy production is more likely to generate detectable enhancements than dispersed beef production, because dairies store manure in lagoons and concentrate emissions in a small area. These contrasts define a detection envelope. Outside it, a weak satellite signal is not evidence of little livestock activity.

This envelope also sets what the satellite can and cannot do. It adds little to continuous herd-size prediction beyond existing inventories and geographic information, and it does not reliably track changes in livestock activity over time. What it does provide is an independent physical signal for screening unusually large, concentrated operations and for checking patterns recorded in administrative data. Its value is greatest where emissions are concentrated, and ground data are sparse. It complements survey infrastructure, not replace it.

6.2 Implications for Agricultural Statistics and Methane Policy

Because we validated satellite methane against official livestock records where ground truth exists, the same observations can help flag large concentrated operations and test the spatial consistency of reported inventories where ground data are limited. This matters most where official statistics lack detail on livestock composition. Our U.S. results show that separating dairy from beef cattle is essential for interpreting the signal, yet such distinctions are rarely available at fine spatial scales. Satellite methane can therefore supplement conventional livestock statistics, but its selective detectability prevents it from replacing a livestock census.

These findings also inform the targeting of methane mitigation. Assessments of the likely exceedance of 1.5°C put rapid methane reductions at the center of any return pathway (United Nations Environment Programme, 2026), raising the value of independent measurement of where livestock methane can and cannot be observed. Large confined operations are both among the most

detectable sources in our analysis and plausible targets for feed additives and manure methane capture (Wang et al., 2024; Beach et al., 2015). Satellite observations can thus complement facility records in flagging areas for further investigation and prioritizing mitigation, including under commitments such as the Global Methane Pledge (Global Methane Pledge, 2021). These uses must respect the detection limits documented here. Identifying concentrated activity is not the same as measuring facility-level emissions or verifying reductions. Current sensors cannot provide comprehensive facility-level monitoring, though higher-resolution instruments may progressively lower the minimum detectable source size.

6.3 Beyond Livestock: Implications for Sensing-Based Economic Measurement

The approach generalizes beyond livestock methane. Any sensing-based indicator of economic activity can be evaluated as a measurement instrument rather than a black box, through four steps: (1) establish that the physical signal co-varies with the activity once broad background variation is removed; (2) distinguish it from co-located alternatives; (3) map the detection envelope; and (4) validate against ground truth where it exists. The same steps apply to other agricultural activities that leave observable physical traces, such as irrigation, tillage, and land-use intensity.

These findings also matter for empirical work that uses remotely sensed variables as proxies for economic activity. When the link between a physical signal and the underlying activity varies across locations and production systems, measurement error may be systematic rather than classical, and such errors can bias subsequent economic estimates (Proctor et al., 2023). Characterizing the detection envelope helps researchers judge where remotely sensed measures are reliable and where measurement error is more consequential. The transferable question is not whether a sensing measure contains useful information, but when.

7 Conclusion

This paper examine whether satellite methane contains useful information about livestock activity globally. We answer with a measurement validity design applied to an eighteen-year global panel, and report three findings. First, satellite methane contains a robust livestock-related spatial signal. Methane concentrations rise with livestock activity worldwide. Second, this signal reveals livestock activity only under identifiable conditions. Detection is strongest when livestock emissions are large relative to the local methane background, as the contrast between concentrated dairy and dispersed beef production and the U.S. facility-level evidence both show. Third, the satellite adds little for continuous herd-size prediction or temporal change, but substantially more for screening and independently verifying large, concentrated livestock operations.

The approach has limitations. The livestock–methane coefficient is a spatial association within neighborhoods, not a causal effect. Placebos and source controls strengthen attribution but cannot rule out every methane-specific confounder, and the Tier 1 measure inherits the uncertainty in emission factors. At about eleven kilometers, GHAP resolves only the largest confined clusters, so

the Central Valley result does not show that current satellites can monitor confined operations in general, and part of that enhancement may reflect topographic trapping that only an atmospheric inversion could separate.

The broader takeaway is methodological. Remote sensing can inform parts of the agricultural economy that conventional surveys capture incompletely, but its value depends on knowing when the underlying physical signal is observable. For livestock methane, that means complementing conventional statistics through selective spatial screening and independent verification rather than replacing livestock censuses. As higher-resolution methane instruments come online, the envelope may expand. More generally, pairing physical signals with economic ground truth and a validity design offers a framework for judging when sensing technologies become useful economic measurements.

References

Beach, Robert H., Jared Creason, Sara Bushey Ohrel, Shaun Ragnauth, Stephen Ogle, Changsheng Li, Pete Ingraham, and William Salas, "Global Mitigation Potential and Costs of Reducing Agricultural Non-CO_2 Greenhouse Gas Emissions through 2030," *Journal of Integrative Environmental Sciences*, 2015, *12* (sup1), 87–105.

Beatty, Lauren, Mei Mei Collins, David McLaughlin, Jasmin Wehner, and Wendong Zhang, "Do Dairy Digesters Reduce Methane Emissions? Evidence from Airborne Remote Sensing," 2026. Working paper, Environmental Defense Fund and Cornell University.

Chen, Tianqi and Carlos Guestrin, "XGBoost: A Scalable Tree Boosting System," in "Proceedings of the 22nd ACM SIGKDD International Conference on Knowledge Discovery and Data Mining" Association for Computing Machinery New York, NY 2016, pp. 785–794.

Conley, Timothy G., "GMM Estimation with Cross Sectional Dependence," *Journal of Econometrics*, 1999, *92* (1), 1–45.

Davis, Kyle Frankel, Weston Anderson, Steffen Ehrmann, Rafaela Flach, Carsten Meyer, Jonathan Proctor, Deepak Ray, Liangzhi You, Michael Foley, Hervé Kerdiles, Andrew Hultgren, Peter Huybers, Endalkachew Kebede, Michele Meroni, Caro Park, and Donghoon Lee, "HarvestStat: A Global Effort towards Open and Standardized Sub-National Agricultural Data," *Environmental Research Letters*, 2025, *20* (5), 052001.

Davitt, Aaron, Derek Tesser, Edward Boyda, Ashutosh Pawar, Omar Al Akkad, Paul Tulloch, Andrew Tulloch, Sam Schiller, Lekha Sridhar, Lauren Betz, and Vasit Sagan, "Agriculture Sector: Cattle Operations — Asset-Level Enteric Fermentation and Manure Management Emissions," Methodology document version 5.4.0, WattTime and Climate TRACE 2026. Accessed 25 October 2026.

Donaldson, Dave and Adam Storeygard, "The View from Above: Applications of Satellite Data in Economics," *Journal of Economic Perspectives*, 2016, *30* (4), 171–198.

Du, Zhenrong, Le Yu, Yue Zhao, Xinyue Li, Xiaoxuan Liu, Xiyu Li, Pengyu Hao, Zhongxin Chen, Zhe Guo, Liangzhi You, Xiaorui Ma, and Hongyu Wang, "Annual Global Gridded Livestock Mapping from 1961 to 2021," *Earth System Science Data*, 2025, *17*, 5543–5566.

Duren, Riley M., Andrew K. Thorpe, Kelsey T. Foster, Talha Rafiq, Francesca M. Hopkins, Vineet Yadav, Brian D. Bue, David R. Thompson, Stephen Conley, Nadia K. Colombi, Christian Frankenberg, Ian B. McCubbin, Michael L. Eastwood, Matthias Falk, Jorn D. Herner, Bart E. Croes, Robert O. Green, and Charles E. Miller, "California's Methane Super-Emitters," *Nature*, 2019, *575* (7781), 180–184.

East, James D., Daniel J. Jacob, Dylan Jervis, Nicholas Balasus, Lucas A. Estrada, Sarah E. Hancock, Melissa P. Sulprizio, John Thomas, Xiaolin Wang, Zichong Chen, Daniel J. Varon, and John R. Worden, "Worldwide Inference of National Methane Emissions by Inversion of Satellite Observations with UNFCCC Prior Estimates," *Nature Communications*, 2025, *16*, 11004.

Food and Agriculture Organization of the United Nations, "FAOSTAT Emissions Database: Enteric Fermentation and Manure Management," https://www.fao.org/faostat/ 2024. Accessed October 2026.

Gerber, Pierre J., Henning Steinfeld, Benjamin Henderson, Anne Mottet, Carolyn Opio, Jeroen Dijkman, Alessandra Falcucci, and Giuseppe Tempio, *Tackling Climate Change through Livestock: A Global Assessment of Emissions and Mitigation Opportunities*, Rome: Food and Agriculture Organization of the United Nations, 2013.

Global Methane Pledge, "Global Methane Pledge," https://www.globalmethanepledge.org 2021. Accessed 25 October 2026.

Hancock, Sarah E., Daniel J. Jacob, Zichong Chen, Hannah Nesser, Aaron Davitt, Daniel J. Varon, Melissa P. Sulprizio, Nicholas Balasus, Lucas A. Estrada, María Cazorla, Laura Dawidowski, Sebastián Diez, James D. East, Elise Penn, Cynthia A. Randles, John Worden, Ilse Aben, Robert J. Parker, and Joannes D. Maasakkers, "Satellite Quantification of Methane Emissions from South American Countries: A High-Resolution Inversion of TROPOMI and GOSAT Observations," *Atmospheric Chemistry and Physics*, 2025, *25* (2), 797–817.

Henderson, J. Vernon, Adam Storeygard, and David N. Weil, "Measuring Economic Growth from Outer Space," *American Economic Review*, 2012, *102* (2), 994–1028.

Intergovernmental Panel on Climate Change, *2006 IPCC Guidelines for National Greenhouse Gas Inventories*, Hayama, Japan: Institute for Global Environmental Strategies, 2006. Eggleston, H. S., Buendia, L., Miwa, K., Ngara, T. & Tanabe, K. (eds).

Jacob, Daniel J., Alexander J. Turner, Joannes D. Maasakkers, Jianxiong Sheng, Kang Sun, Xiong Liu, Kelly Chance, Ilse Aben, Jason McKeever, and Christian Frankenberg, "Satellite Observations of Atmospheric Methane and Their Value for Quantifying Methane Emissions," *Atmospheric Chemistry and Physics*, 2016, *16* (22), 14371–14396.

Jean, Neal, Marshall Burke, Michael Xie, W. Matthew Davis, David B. Lobell, and Stefano Ermon, "Combining Satellite Imagery and Machine Learning to Predict Poverty," *Science*, 2016, *353* (6301), 790–794.

Lauvaux, Thomas, Clement Giron, Matthieu Mazzolini, Alexandre d'Aspremont, Riley Duren, Daniel Cusworth, Drew Shindell, and Philippe Ciais, "Global Assessment of Oil and Gas Methane Ultra-Emitters," *Science*, 2022, *375* (6580), 557–561.

Lobell, David B., "The Use of Satellite Data for Crop Yield Gap Analysis," *Field Crops Research*, 2013, *143*, 56–64.

Lundberg, Scott M. and Su-In Lee, "A Unified Approach to Interpreting Model Predictions," in Isabelle Guyon, Ulrike von Luxburg, Samy Bengio, Hanna Wallach, Rob Fergus, S. V. N. Vishwanathan, and Roman Garnett, eds., *Advances in Neural Information Processing Systems 30*, Curran Associates Red Hook, NY 2017, pp. 4765–4774.

Park, Caro, Jonathan Proctor, and Peter Huybers, "Divergent Estimates of Agricultural Climate Sensitivity from Survey and Satellite Yield Data," *Environmental Research Letters*, 2026, *21* (15), 154044.

Parker, Robert J., Alex Webb, Hartmut Boesch, Peter Somkuti, Rocio Barrio Guillo, Antonio Di Noia, Nikoleta Kalaitzi, Jasdeep S. Anand, Peter Bergamaschi, Frederic Chevallier, Paul I. Palmer, Liang Feng, Nicholas M. Deutscher, Dietrich G. Feist, David W. T. Griffith, Frank Hase, Rigel Kivi, Isamu Morino, Justus Notholt, Young-Suk Oh, Hirofumi Ohyama, Christof Petri, David F. Pollard, Coleen Roehl, Mahesh K. Sha, Kei Shiomi, Kimberly Strong, Ralf Sussmann, Yao Té, Voltaire A. Velazco, Thorsten Warneke, Paul O. Wennberg, and Debra Wunch, "A Decade of GOSAT Proxy Satellite CH_4 Observations," *Earth System Science Data*, 2020, *12* (4), 3383–3412.

Proctor, Jonathan, Tamma Carleton, and Sandy Sum, "Parameter Recovery Using Remotely Sensed Variables," Working Paper 30861, National Bureau of Economic Research, Cambridge, MA 2023.

_ , _ , Trinetta Chong, Taryn Fransen, Simon Greenhill, Jessica Katz, Hikari Murayama, Luke Sherman, Jeanette Tseng, Hannah Druckenmiller, and Solomon Hsiang, "What Can Satellite Imagery and Machine Learning Measure?," Working Paper 34315, National Bureau of Economic Research, Cambridge, MA 2025.

Qu, Yu, Jing Wei, Hanfa Xing, Xian Shi, Zurui Ao, and Xiaoliang Meng, "Global Estimates of Daily Gapless Atmospheric XCH_4 Concentrations from Satellite and Reanalysis Data During 2003–2020," *IEEE Transactions on Geoscience and Remote Sensing*, 2025, *63*, 1–12.

Reuland, Frances E., Taylor Adams, Evan D. Sherwin, Sahar H. El Abbadi, Eric A. Kort, and Adam R. Brandt, "Evaluating Space-Based Methane Detection through a One-Year Blind Test," *Nature*, 2026, *658*, 673–681.

Roberts, David R., Volker Bahn, Simone Ciuti, Mark S. Boyce, Jane Elith, Gurutzeta Guillera-Arroita, Severin Hauenstein, José J. Lahoz-Monfort, Boris Schröder, Wilfried Thuiller, David I. Warton, Brendan A. Wintle, Florian Hartig, and Carsten F. Dormann, "Cross-Validation Strategies for Data with Temporal, Spatial, Hierarchical, or Phylogenetic Structure," *Ecography*, 2017, *40* (8), 913–929.

Rossi-Hansberg, Esteban and Jialing Zhang, "Local GDP Estimates Around the World," *Journal of Urban Economics*, 2026, *154*, 103871.

Saunois, Marielle, Adrien Martinez, Benjamin Poulter, Zhen Zhang, Peter A. Raymond, Pierre Regnier, Josep G. Canadell, Robert B. Jackson, Prabir K. Patra, Philippe Bousquet, Philippe Ciais, Edward J. Dlugokencky, Xin Lan, George H. Allen, David Bastviken, David J. Beerling, Dmitry A. Belikov, Donald R. Blake, Simona Castaldi, Monica Crippa, Bridget R. Deemer, Fraser Dennison, Giuseppe Etiope, Nicola Gedney, Lena Höglund-Isaksson, Meredith A. Holgerson, Peter O. Hopcroft, Gustaf Hugelius, Akihiko Ito, Atul K. Jain, Rajesh Janardanan, Matthew S. Johnson, Thomas Kleinen, Paul B. Krummel, Ronny Lauerwald, Tingting Li, Xiangyu Liu, Kyle C. McDonald, Joe R. Melton, Jens Mühle, Jurek Müller, Fabiola Murguia-Flores, Yosuke Niwa, Sergio Noce, Shufen Pan, Robert J. Parker, Changhui Peng, Michel Ramonet, William J. Riley, Gerard Rocher-Ros, Judith A. Rosentreter, Motoki Sasakawa, Arjo Segers, Steven J. Smith, Emily H. Stanley, Joël Thanwerdas, Hanqin Tian, Aki Tsuruta, Francesco N. Tubiello, Thomas S. Weber, Guido R. van der Werf, Douglas E. J. Worthy, Yi Xi, Yukio Yoshida, Wenxin Zhang, Bo Zheng, Qing Zhu, Qiuan Zhu, and Qianlai Zhuang, "Global Methane Budget 2000–2020," *Earth System Science Data*, 2025, *17* (5), 1873–1958.

Scarpelli, Tia R., Daniel J. Jacob, Shayna Grossman, Xiao Lu, Zhen Qu, Melissa P. Sulprizio, Yuzhong Zhang, Frances Reuland, Deborah Gordon, and John R. Worden, "Updated Global Fuel Exploitation Inventory (GFEI) for Methane Emissions from the Oil, Gas, and Coal Sectors: Evaluation with Inversions of Atmospheric Methane Observations," *Atmospheric Chemistry and Physics*, 2022, *22* (5), 3235–3249.

United Nations Environment Programme, "Limiting overshoot: navigating exceedance of 1.5°C and pathways towards return," Technical Report, United Nations Environment Programme, Nairobi 2026.

Varon, Daniel J., Dylan Jervis, Jason McKeever, Ian Spence, David Gains, and Daniel J. Jacob, "High-Frequency Monitoring of Anomalous Methane Point Sources with Multispectral Sentinel-2 Satellite Observations," *Atmospheric Measurement Techniques*, 2021, *14* (4), 2771–2785.

Wang, Yue, Zhiping Zhu, Hongmin Dong, Xiuming Zhang, Sitong Wang, and Baojing Gu, "Mitigation Potential of Methane Emissions in China's Livestock Sector Can Reach One-Third by 2030 at Low Cost," *Nature Food*, 2024, *5* (7), 603–614.

Worden, John R., Sudhanshu Pandey, Yuzhong Zhang, Daniel H. Cusworth, Zhen Qu, A. Anthony Bloom, Shuang Ma, Joannes D. Maasakkers, Brendan Byrne, Riley Duren, David Crisp, Deborah Gordon, and Daniel J. Jacob, "Verifying Methane Inventories and Trends with Atmospheric Methane Data," *AGU Advances*, 2023, *4* (4), e2023AV000871.

Wuepper, David, Wyclife Agumba Oluoch, and Hadi Hadi, "Satellite Data in Agricultural and Environmental Economics: Theory and Practice," *Agricultural Economics*, 2025, *56*, 493–511.

Xu, Xiaoming, Prateek Sharma, Shijie Shu, Tzu-Shun Lin, Philippe Ciais, Francesco N. Tubiello, Pete Smith, Nelson Campbell, and Atul K. Jain, "Global Greenhouse Gas Emissions from Animal-Based Foods Are Twice Those of Plant-Based Foods," *Nature Food*, 2021, *2* (9), 724–732.

Yang, Anton, Jianwei Ai, and Costas Arkolakis, "A Geospatial Approach to Measuring Economic Activity," Working Paper 33619, National Bureau of Economic Research, Cambridge, MA 2025. Nature Communications, forthcoming.

Measuring Livestock from Space: Global and U.S. Evidence on the Detection, Attribution, and Limits of Satellite Methane

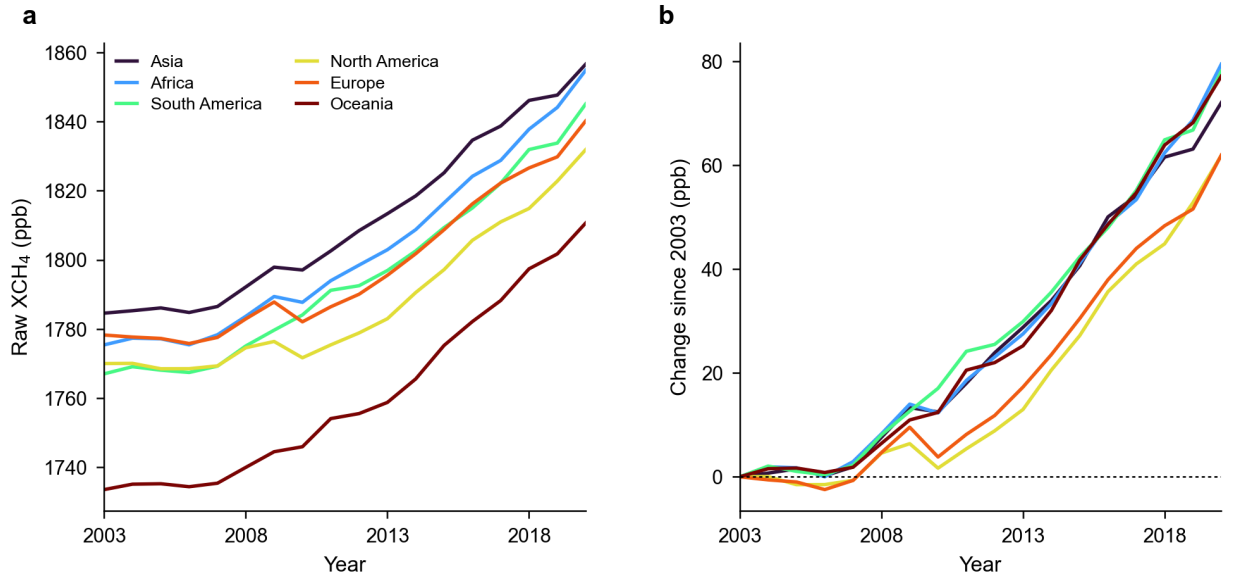
Jianwei Ai Qinan Lu Wendong Zhang

Online Appendix

A1 Data Construction and Descriptive Evidence

A1.1 Satellite Methane Data

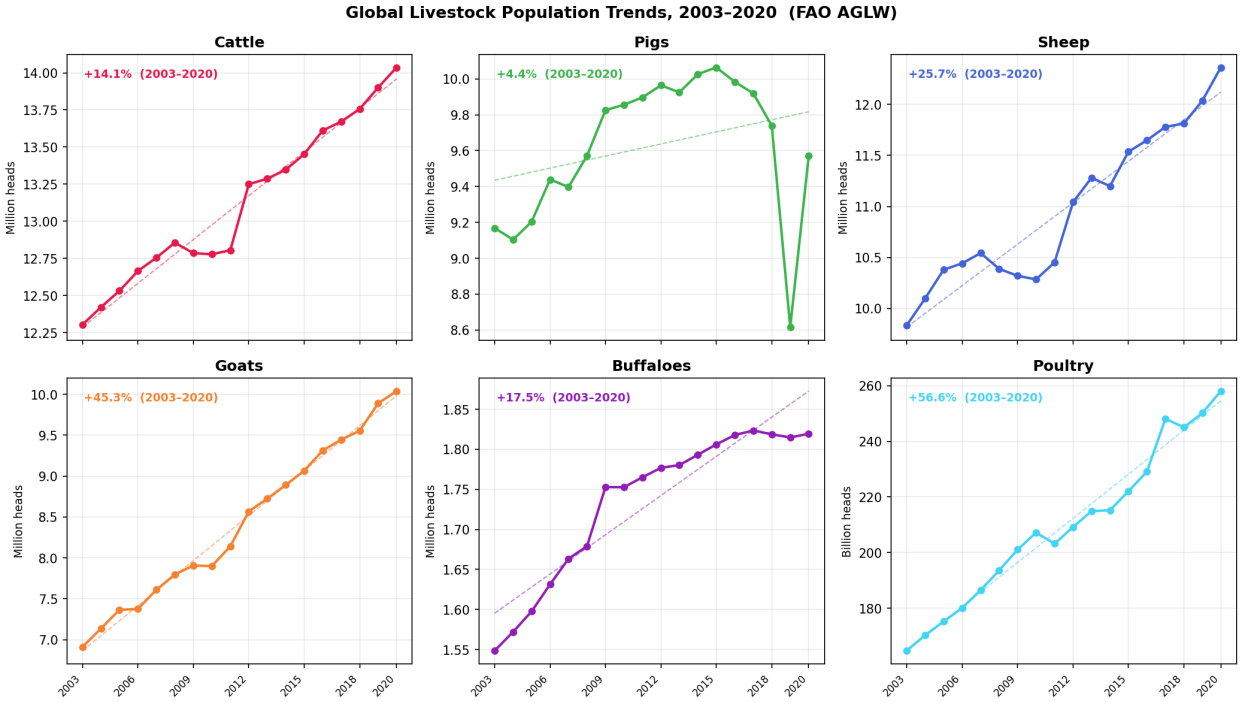
Figure A1. Raw column methane by region and year



Notes: This figure shows the average satellite methane levels for each continent from 2003 to 2020. Panel (a) displays total methane levels. Asia has the highest levels, and Oceania has the lowest levels throughout the entire period. Panel (b) shows the change in methane levels on each continent since 2003. On every continent, methane increased by 60 to 80 parts per billion. The permanent differences in methane levels between continents are caused by general geographic factors rather than livestock activity. Source: GHAP.

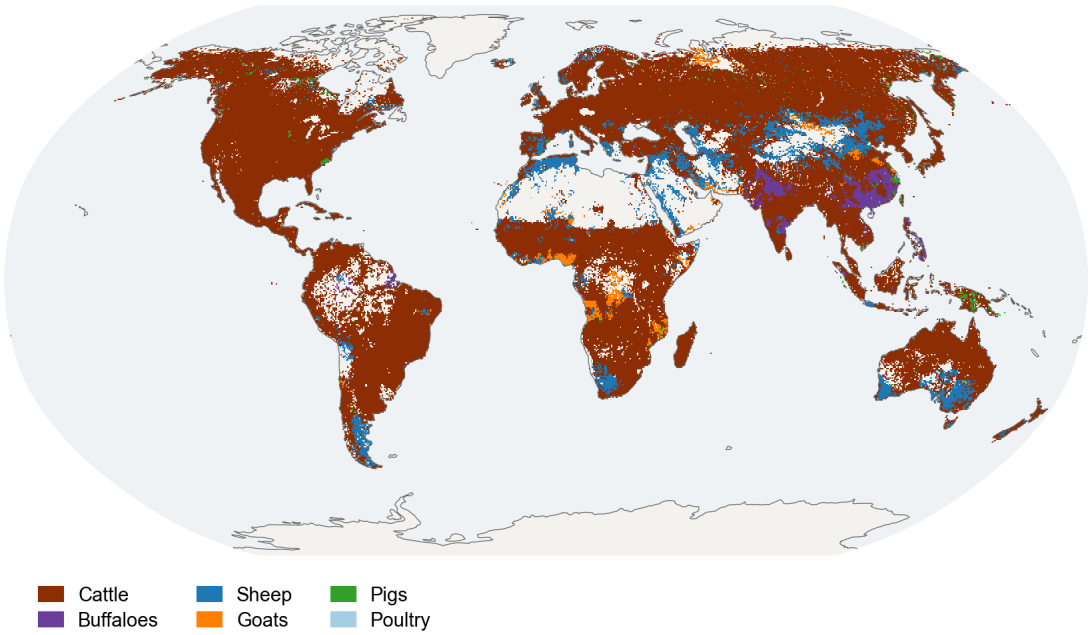
A1.2 Livestock Data and Emission Factors

Figure A2. Livestock head counts by species, 2003 to 2020



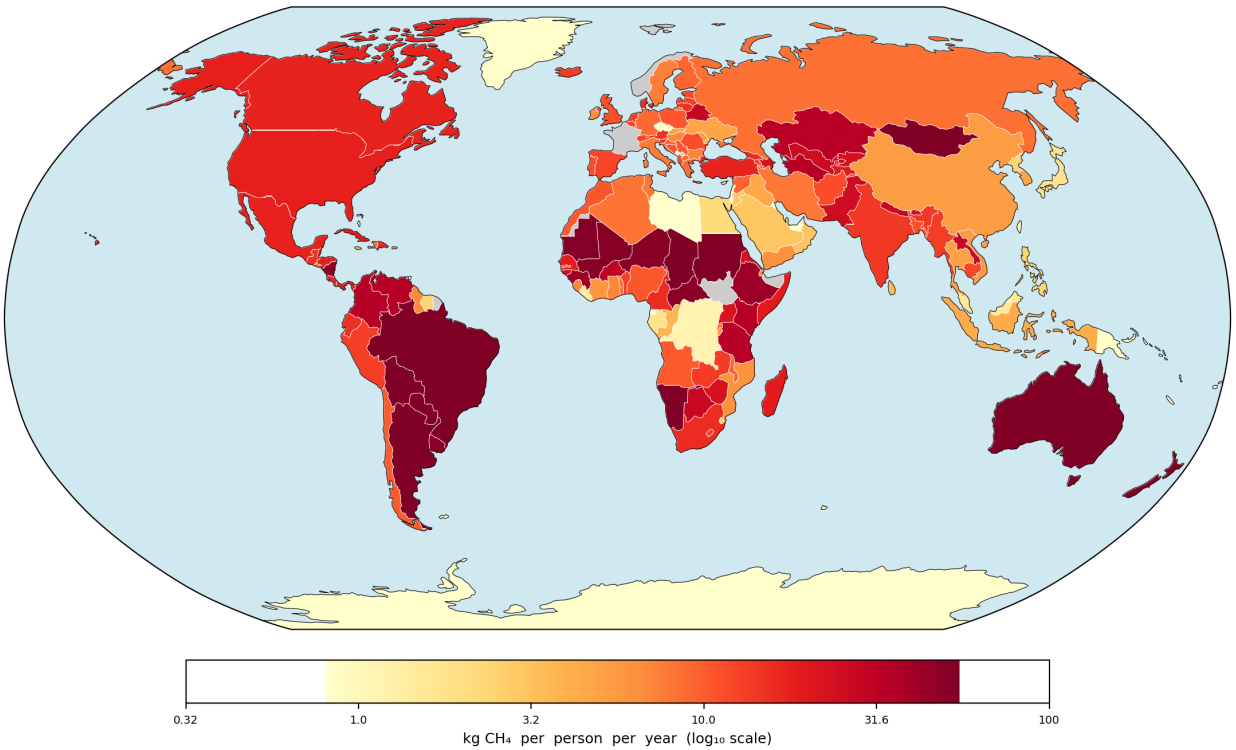
Notes: Global headcounts from AGLW. Poultry and goats grew fastest in proportional terms. Source: AGLW.

Figure A3. Dominant emitting species by cell, 2020



Notes: This figure shows which livestock species produce the most methane in each 0.1° cell. Data are combined into 0.4° blocks to make the map easier to read. Cattle are the primary source of methane in 86 percent of livestock areas. Sheep are the main source in nine percent of areas, primarily in Central Asia, Australia, and Patagonia. Goats and buffaloes are each the main source in two percent of areas. Buffaloes are concentrated in the Indo-Gangetic Plain, while goats are common across the Sahel and Arabia. Sources: AGLW and IPCC.

Figure A4. Livestock methane per person, 2020



Notes: Tier 1 methane divided by national population, on a log scale. Values reflect relative pattern rather than calibrated levels. Source: AGLW and Natural Earth population.

Table A1. Global livestock methane by species, Tier 1

Species	2003 (Mt)	2020 (Mt)	Head count growth
Cattle	80.3	93.8	+17%
Buffaloes	9.5	11.1	+17%
Sheep	7.9	10.1	+29%
Goats	3.8	5.6	+48%
Pigs	1.3	1.4	+5%
Poultry	0.3	0.5	+59%
Total	**103.1**	**122.6**	+18.9%

Notes: Full grid AGLW head counts times IPCC 2006 Tier 1 emission factors. The gridded head counts match FAO, for example 1.51 billion cattle in 2020 against about 1.53 billion. Cattle are 76.5 percent of the 2020 total. Emission factors: cattle 62, buffaloes 55, sheep 8, goats 5, pigs 1.5, poultry 0.02 kilograms of methane per head per year. Source: AGLW and IPCC 2006 guidelines.

A1.3 Additional Data Sources

Table A2. Overview of data sources, coverage, and empirical roles

Dataset	Period	Resolution	Role
GHAP XCH_4	2003–2020	0.1°	Satellite methane, main outcome
GHAP XCO_2	2003–2020	0.1°	Biogenic ratio fingerprint
GHAP surface O_3	2019	0.1°	Placebo outcome
AGLW livestock	2003–2020	0.1°	Livestock activity
GlobalRice20	2015	0.1°	Rice confounder
GFEI oil/gas/coal	2019	0.1°	Fossil confounder (direct)
EDGAR v2025 waste	2020	0.1°	Landfill, wastewater
EDGAR v2025 CH_4 total	2003–2020	0.1°	Total methane reference
USDA NASS QuickStats	2003–2020	State/nation	U.S. cattle and hog inventory
USDA county cattle panel	2000–2024	County	U.S. dairy and beef cattle
BLS price indices	2003–2020	National	U.S. livestock and food prices
FAOSTAT emissions	2003–2020	Country	Enteric and manure split by species

Notes: GHAP is from GlobalHighAirPollutants (GHAP). Sentinel 5P TROPOMI and ECMWF EAC4 were considered but are not used in the main analysis. Source: as listed.

Table A3. Summary statistics for the global livestock–methane sample

Variable	Mean	SD	p10	p50	p90
Panel A. 2019 (main analysis year)					
Satellite outcomes					
Raw XCH_4 (ppb)	1,837.34	19.75	1,815.75	1,836.74	1,860.83
Raw XCO_2 (ppm)	408.90	1.15	407.15	408.87	410.21
Surface O_3 (ppb)	36.16	5.81	30.10	35.30	43.90
Livestock					
Livestock CH_4 (kt per cell)	0.118	0.251	0.000	0.028	0.321
Log livestock CH_4	9.73	2.61	5.71	10.25	12.68
Animal units per cell	1,725	3,571	4	423	4,820
Cattle (head per cell)	1,442	2,953	4	309	4,182
Buffaloes (head per cell)	226	1,774	0	0	2
Sheep (head per cell)	1,169	3,167	0	63	3,541
Goats (head per cell)	1,087	3,850	0	24	2,855
Pigs (head per cell)	715	3,486	0	0	1,127
Poultry (head per cell)	18,898	96,396	0	0	30,809
Confounder controls					
Rice fraction (percent)	16.91	37.48	0.00	0.00	100.00
Fossil CH_4 (Mg km^{-2} yr^{-1})	1.030	26.381	0.000	0.002	0.212
Waste CH_4 (t per cell yr^{-1})	43.00	1,196.85	0.00	0.00	14.67
Observations	647,529 cells				
Panel B. 2020 (most recent year)					
Satellite outcomes					
Raw XCH_4 (ppb)	1,847.98	20.87	1,822.21	1,847.52	1,873.32
Raw XCO_2 (ppm)	410.97	1.14	409.07	411.21	412.08
Surface O_3 (ppb)	35.16	5.85	29.40	34.30	43.30
Livestock					
Livestock CH_4 (kt per cell)	0.126	0.258	0.000	0.032	0.346
Log livestock CH_4	9.85	2.58	5.83	10.39	12.75
Animal units per cell	1,855	3,675	4	489	5,209
Cattle (head per cell)	1,562	3,105	5	357	4,551
Buffaloes (head per cell)	227	1,768	0	0	5
Sheep (head per cell)	1,182	3,249	0	65	3,500
Goats (head per cell)	1,095	3,906	0	26	2,867
Pigs (head per cell)	834	3,841	0	0	1,271
Poultry (head per cell)	20,805	93,321	0	11	36,736
Confounder controls					
Rice fraction (percent)	18.48	38.82	0.00	0.00	100.00
Fossil CH_4 (Mg km^{-2} yr^{-1})	1.030	26.918	0.000	0.002	0.217
Waste CH_4 (t per cell yr^{-1})	45.50	1,172.82	0.00	0.00	17.60
Observations	659,167 cells				

Notes: The sample consists of land cells with positive livestock density and observed satellite methane, corresponding to the sample used in the global livestock–methane gradient analysis. Panel A reports summary statistics for 2019, the main analysis year, and Panel B reports statistics for 2020, the final year of the satellite record. Satellite variables are raw retrieved values without background removal; neighborhood fixed effects account for broad spatial variation in atmospheric background in the regression analysis. Species counts are measured as heads per 0.1° grid cell and are constructed by multiplying AGLW livestock densities by cell area. Livestock CH_4 applies IPCC Tier 1 emission factors to these counts.

A2 Alternative Spatial Specifications

A2.1 Spatially Robust Inference

Raw XCH_4 is strongly spatially autocorrelated, so inference that assumes independence across cells would be badly miscalibrated. We report three schemes. The baseline clusters standard errors by 5° neighborhood, which allows arbitrary dependence within blocks. We add Conley spatial heteroskedasticity and autocorrelation-consistent standard errors (Conley, 1999), which allow dependence that decays with distance. Writing the residualized regressor as $\tilde{x}_i$ and the residual as $\hat{\varepsilon}_i$, and letting $K(d_{ij})$ be a uniform kernel equal to one when the distance d_{ij} between cells is below a cutoff and zero otherwise, the Conley variance of $\hat{\beta}$ is

$$\widehat{\mathrm{Var}}(\hat{\beta}) = \Big(\textstyle\sum_i \tilde{x}_i^2 \Big)^{-2} \sum_i \sum_j K(d_{ij})\, \tilde{x}_i \hat{\varepsilon}_i\, \tilde{x}_j \hat{\varepsilon}_j, \tag{4}$$

which we evaluate at cutoffs of 200 and 500 kilometers. Because the cells lie on a regular grid, we compute the double sum efficiently by convolving the cell-level score $\tilde{x}_i \hat{\varepsilon}_i$ with a disk kernel, which avoids forming the full pairwise distance matrix. We also report a spatial block bootstrap that resamples whole neighborhoods with replacement, which makes no parametric assumption about the dependence structure (Roberts et al., 2017). And as a falsification test, we permute $\log \ell_i$ within neighborhoods and re-estimate, since a valid gradient should vanish when the livestock labels are scrambled.

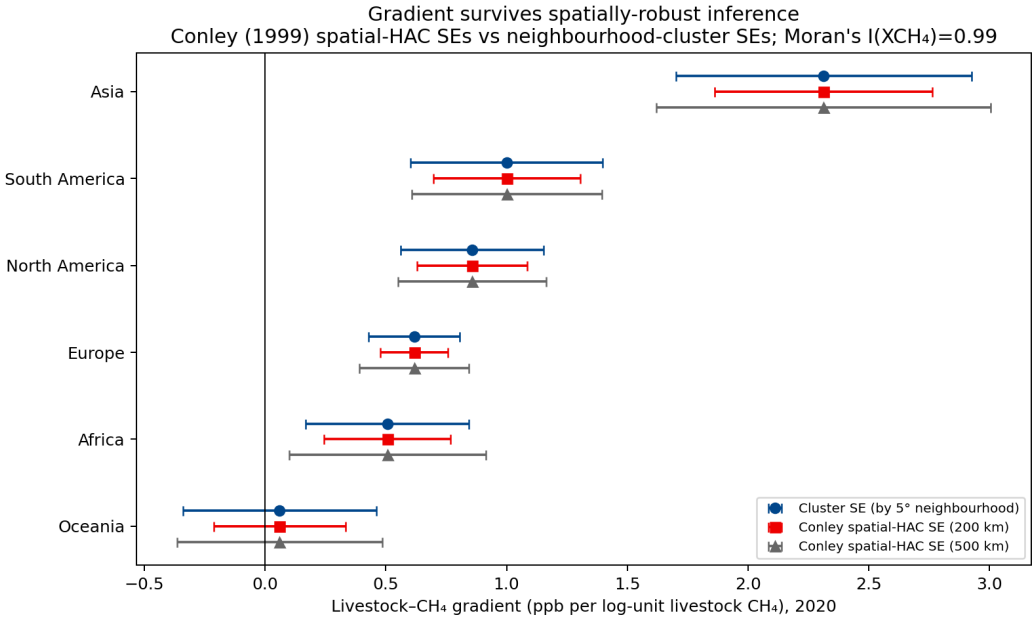
Figure A5 reports the gradient with confidence intervals under neighborhood cluster standard errors and under Conley spatial standard errors at 200 and 500 kilometers. The gradient remains significant on five of six continents even at the 500-kilometer cutoff, and the cluster and Conley 500-kilometer errors are similar in magnitude, which validates the cluster approach used in the main tables.

Table A4. The spatial livestock methane coefficient by continent, 2019

Continent	Coefficient	Cluster SE	Conley 500 km SE	With controls	n
Asia	2.31	0.29	0.33	1.83	114,159
South America	1.14	0.25	0.23	1.16	52,624
North America	0.72	0.12	0.12	0.68	128,455
Europe	0.57	0.09	0.10	0.48	181,317
Africa	0.50	0.16	0.19	0.44	126,451
Oceania	0.06	0.25	0.27	0.06	44,523

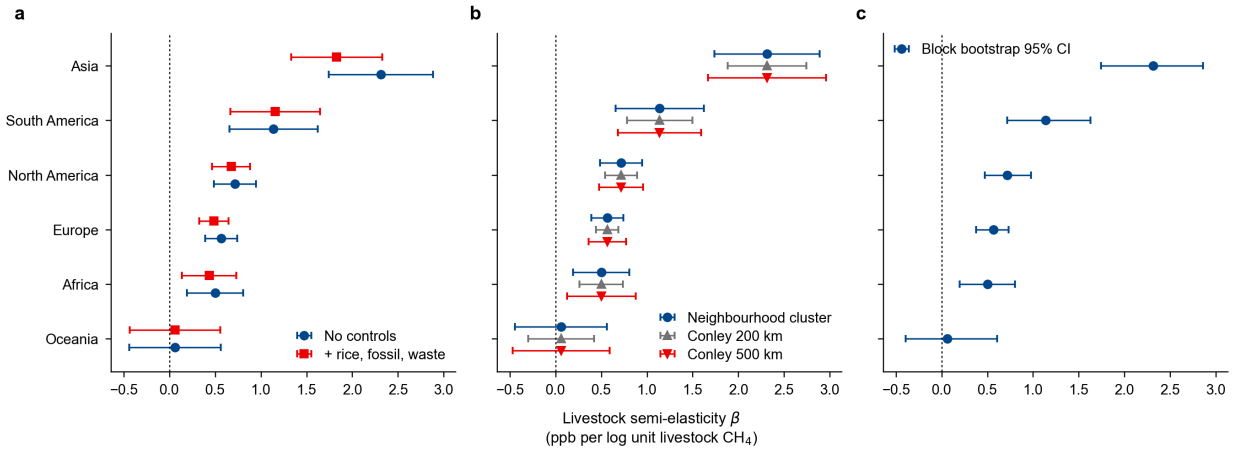
Notes: Estimate of β from Equation (1), in parts per billion per log unit of livestock methane. The outcome is raw XCH_4; the 5° by 5° neighborhood fixed effects remove the background in one step. Standard errors: cluster robust by neighborhood, and Conley spatial at a 500-kilometer cutoff. The confounder column adds rice, direct oil, gas, and coal methane from GFEI, and landfill and wastewater methane from EDGAR. A permutation placebo that reshuffles livestock within neighborhoods yields coefficients near zero on every continent. Source: GHAP and AGLW.

Figure A5. Conley spatial standard errors



Notes: The gradient with 95 percent intervals under cluster and Conley spatial errors. Source: GHAP and AGLW.

Figure A6. The livestock semi-elasticity by continent, and its robustness



Notes: This figure reports the estimated effects of livestock on methane for each continent in 2019. All results include 95 percent confidence intervals and use a consistent horizontal scale. Panel (a) shows the findings with and without accounting for other methane sources, such as rice farming, oil, gas, coal, landfills, and wastewater. Panel (b) compares different ways of measuring the accuracy of these results using standard regional methods and geographic ranges of 200 and 500 kilometers. Panel (c) shows results from a "bootstrap" test that re-examines the data 400 times by resampling different neighborhoods. The relationship between livestock and methane is positive on five of the six continents studied and remains strong regardless of the testing method used. Accounting for other methane sources slightly reduces the effect, confirming that the signal is driven by livestock rather than by fossil fuels or waste. Sources: GHAP, AGLW, GlobalRice20, GFEI, and EDGAR (version 2025).

Table A5. The livestock methane coefficient

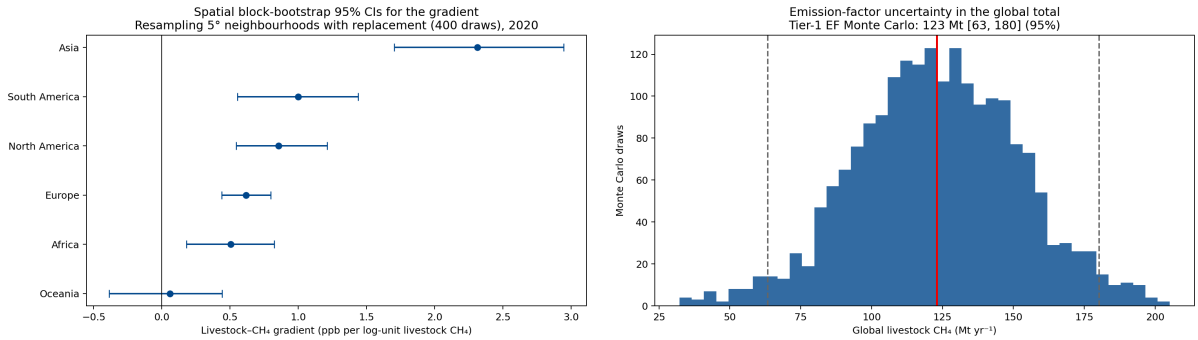
	(1)	(2)	(3)	(4)	(5)
Log livestock CH_4	0.791***	0.753***	0.689***	0.504***	1.239***
	(0.071)	(0.067)	(0.064)	(0.041)	(0.164)
Rice control	No	Yes	Yes	Yes	Yes
Fossil control	No	No	Yes	Yes	Yes
Waste control	No	No	Yes	Yes	Yes
Neighborhood FE	5°	5°	5°	3°	10°
Observations	647,529	647,529	647,529	647,529	647,529
Neighborhoods	754	754	754	1,826	233
Within R^2	0.045	0.060	0.078	0.057	0.132

Notes: Pooled estimate of β on log Tier 1 livestock methane with neighborhood fixed effects, 2019. Column 1 is the baseline; columns 2 and 3 add the confounder controls; columns 4 and 5 vary the fixed effect block size. Pooled OLS of raw XCH_4 on log Tier 1 livestock methane with neighborhood fixed effects, 2019 land sample. Cluster robust standard errors by the neighborhood block in parentheses. Controls are log rice fraction, log GFEI fossil methane, and log EDGAR waste methane. The pooled slope averages across continents; Table A4 reports the heterogeneity by continent. $^{*}p < 0.1$, $^{**}p < 0.05$, $^{***}p < 0.01$. Source: GHAP, AGLW, GlobalRice20, GFEI, EDGAR.

A2.2 Sampling Uncertainty

Figure A7 reports the spatial block bootstrap distribution of the gradient and the Tier 1 emission factor Monte Carlo distribution of the global total. The bootstrap confidence interval excludes zero on five of six continents. The emission factor Monte Carlo makes explicit that the absolute total is uncertain, at 123 megatons with a 95 percent interval of 63 to 180.

Figure A7. Bootstrap and Monte Carlo uncertainty

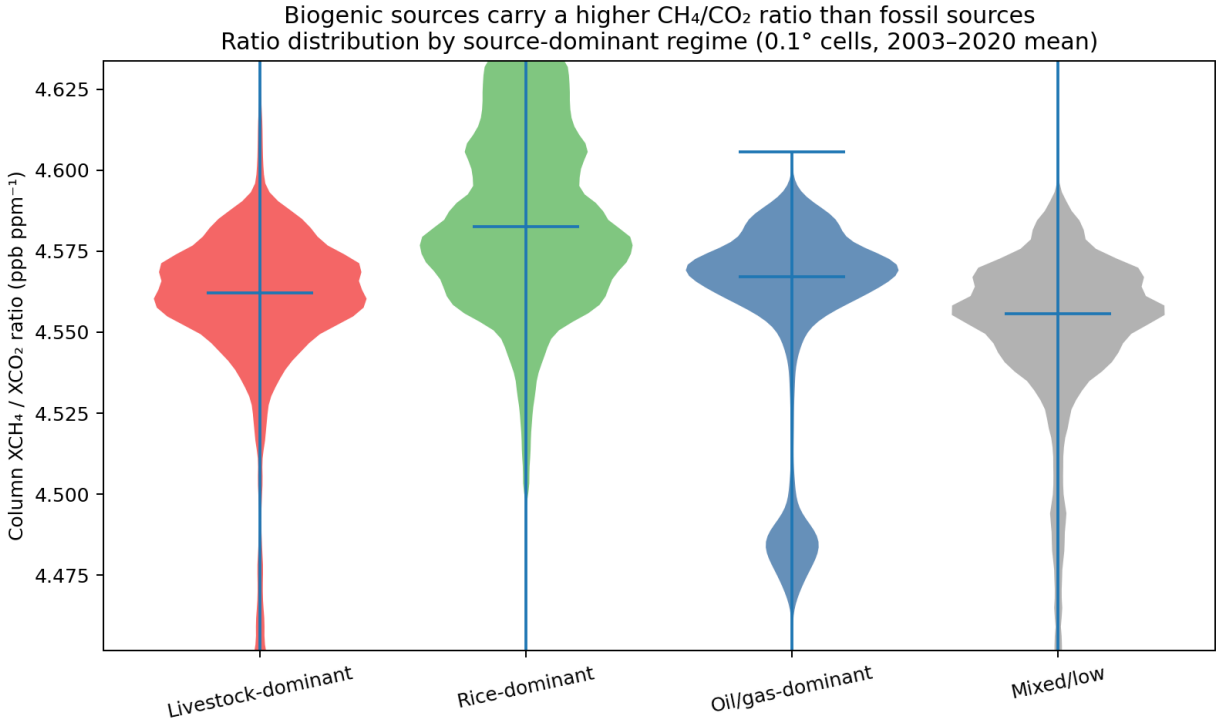


Notes: Left, spatial block bootstrap intervals for the gradient. Right, emission factor Monte Carlo for the global total. Source: GHAP, AGLW, IPCC 2006 factors.

A3 Attribution and Atmospheric Placebos

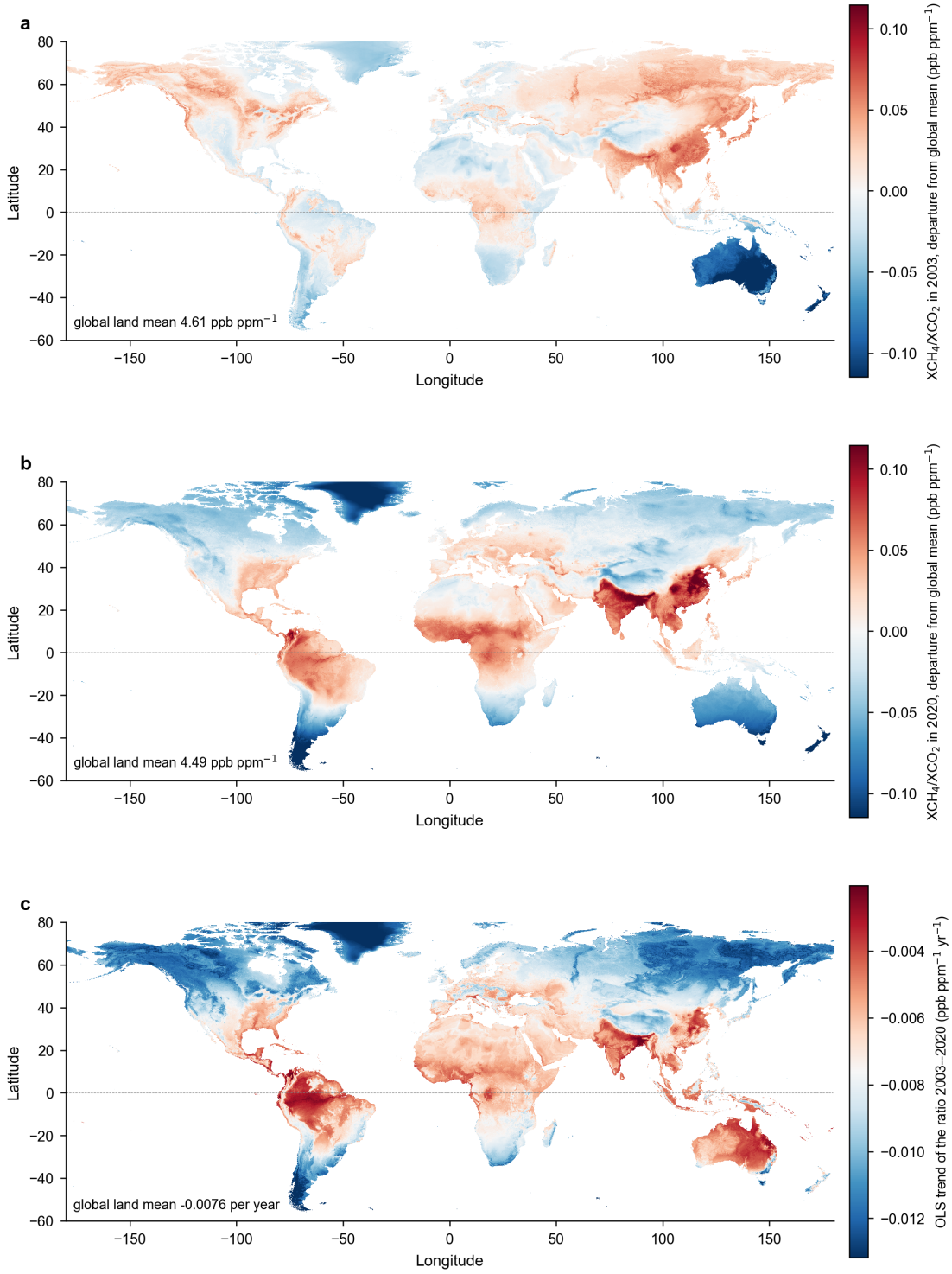
Figure A8 shows the distribution of the ratio across cells classified by dominant source, and Figure A9 maps the ratio in 2003 and 2020 and its change. The ratio is higher over rice and livestock regions, which are biogenic, than over oil and gas regions, consistent with a biogenic origin for the local enhancements, though the absolute differences are small because the signal is column integrated.

Figure A8. Methane to carbon dioxide ratio by source regime



Notes: Distribution of the column ratio across cells classified as rice, livestock, or oil and gas dominant. Source: GHAP XCH_4 and XCO_2.

Figure A9. Methane to carbon dioxide ratio, levels and change



Note: The ratio in 2003 and 2020 and its change. Source: GHAP XCH_4 and XCO_2.

Table A6. Pollutant placebo: the coefficient is specific to methane

	Outcome pollutant (SD units)			Methane
Continent	Methane	Carbon dioxide	Ozone	controlling CO_2 (ppb)
All	0.219^{***}	0.136^{***}	0.037^{**}	0.47^{***}
Asia	0.431^{***}	0.298^{***}	0.188^{***}	1.19^{***}
South America	0.266^{***}	0.192^{***}	-0.137^{*}	0.62^{***}
North America	0.225^{***}	0.190^{***}	-0.004	0.25^{***}
Europe	0.218^{***}	0.101^{***}	0.010	0.38^{***}
Africa	0.156^{***}	0.038	0.082^{*}	0.45^{***}
Oceania	0.023	-0.043	-0.117	0.12

Notes: Each entry is the coefficient on log Tier 1 livestock methane from the main specification, raw concentration with 5° neighborhood fixed effects and neighborhood clustered standard errors, 2019, estimated on the identical sample of 647,508 cells. Coefficients are expressed in within-neighborhood standard deviations of the outcome so that the pollutants are comparable. The final column adds raw XCO_2 as a control to the methane regression.

A4 Machine Learning and Model Performance

A4.1 Shapley Value

We compute Shapley values, which allocate the model prediction across features in a way that is additive and consistent, and we rank features by mean absolute Shapley value as a measure of importance (Lundberg and Lee, 2017). The unique additive attribution satisfying efficiency, symmetry, and consistency:

$$\hat{f}(x_i) = \phi_0 + \sum_{k=1}^{12} \phi_{ik}, \qquad \phi_{ik} = \sum_{S \subseteq K \setminus \{k\}} \frac{|S|!\,(|K| - |S| - 1)!}{|K|!} \left[\hat{f}_S(x_{iS}) - \hat{f}_{S\setminus\{k\}}(x_{i,S\setminus\{k\}})\right], \tag{5}$$

where K is the feature set, $\hat{f}_S$ the model's expectation conditional on the features in S, and ϕ_0 the mean prediction. For tree ensembles, the exact values are computable in polynomial time (Lundberg and Lee, 2017), and we use that estimator on a random 60,000-cell subsample of the fitted model. The importance we report for feature k is the mean absolute Shapley value, $\bar{\phi}_k = \frac{1}{n}\sum_i |\phi_{ik}|$, in parts per billion. We measure the importance of each factor as its average absolute Shapley value. This metric represents the average amount, measured in parts per billion, that a specific factor moves the predicted methane level away from the overall average.

A4.2 Metrics of Model Performance

Table A7. Predictive skill for the local methane residual is low on every metric

Model	R^2	RMSE	MAE	Median AE	MAPE (%)	Bias
Mean baseline	0.000	3.95	2.87			0.000
OLS	0.052	3.85	2.82	2.10	96.6	0.000
Ridge	0.071	3.81	2.81	2.09	97.1	0.000
Lasso	0.070	3.81	2.81	2.09	97.0	0.000
Random forest	0.495	2.81	2.00	1.42	70.3	0.020
Histogram GBM	0.577	2.57	1.84	1.32	65.0	0.015
Gradient boosted trees	0.587	2.54	1.81	1.30	63.8	0.021

Notes: The variable we predict is a difference centered at zero. Because percentage errors cannot be calculated when the true value is zero, we report the mean absolute percentage error only for areas where this difference is at least one part per billion. We also tested two alternative samples of 300,000 areas, both of which resulted in lower model accuracy. When we include all 18 years of data, the accuracy is 0.45. When we include the 36 percent of land areas that have no livestock, the accuracy falls to 0.37. This decrease occurs because the model cannot use livestock data to explain methane levels in areas where no animals are present. Sources: GHAP, AGLW, GlobalRice20, GFEI, and EDGAR.

A5 Livestock Accounting Detail

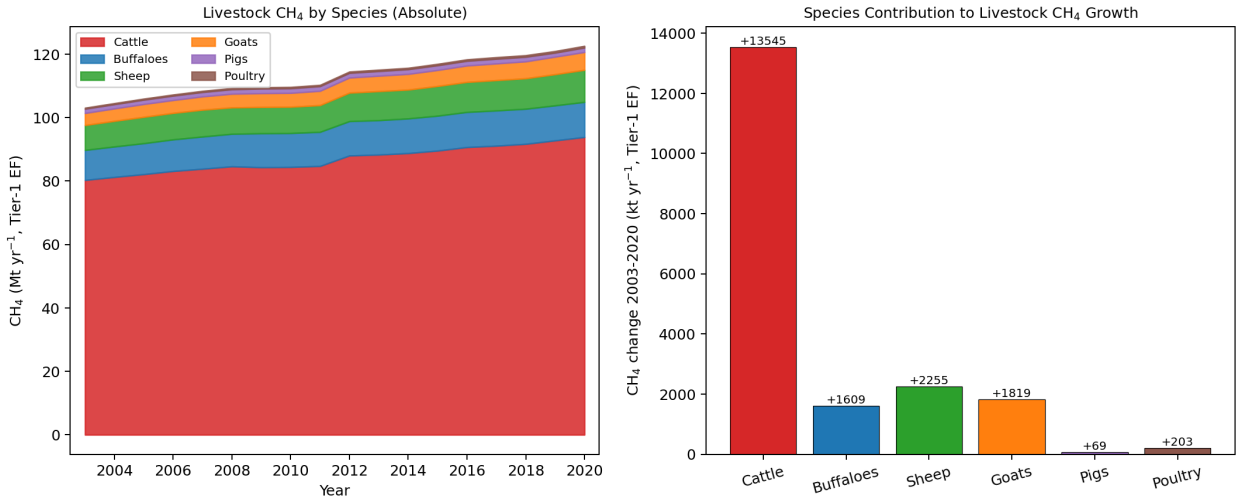
We compute Tier 1 livestock methane from the gridded census as follows. For each 0.1° cell i and species s, the head count is the AGLW animal density times the cell area, $N_{s,i} = D_{s,i}\, A_i$, where $A_i = (111 \times 0.1)^2 \cos\phi_i$ square kilometers corrects for the convergence of the meridians at latitude ϕ_i. Livestock methane in the cell is the head count weighted sum of the IPCC 2006 Tier 1 emission factors,

$$M_i = \sum_s N_{s,i}\, \mathrm{EF}_s, \qquad \mathrm{EF} = (62,\ 55,\ 8,\ 5,\ 1.5,\ 0.02)\ \text{kg CH}_4\ \text{head}^{-1}\ \text{yr}^{-1}, \tag{6}$$

for cattle, buffaloes, sheep, goats, pigs, and poultry, respectively, each factor combining enteric fermentation and manure management (Intergovernmental Panel on Climate Change, 2006). Global and national totals sum M_i over the full grid, and the per capita map divides the national total by population. Equation (6) is the quantity mapped in Figures A4 and tabulated in Table A1.

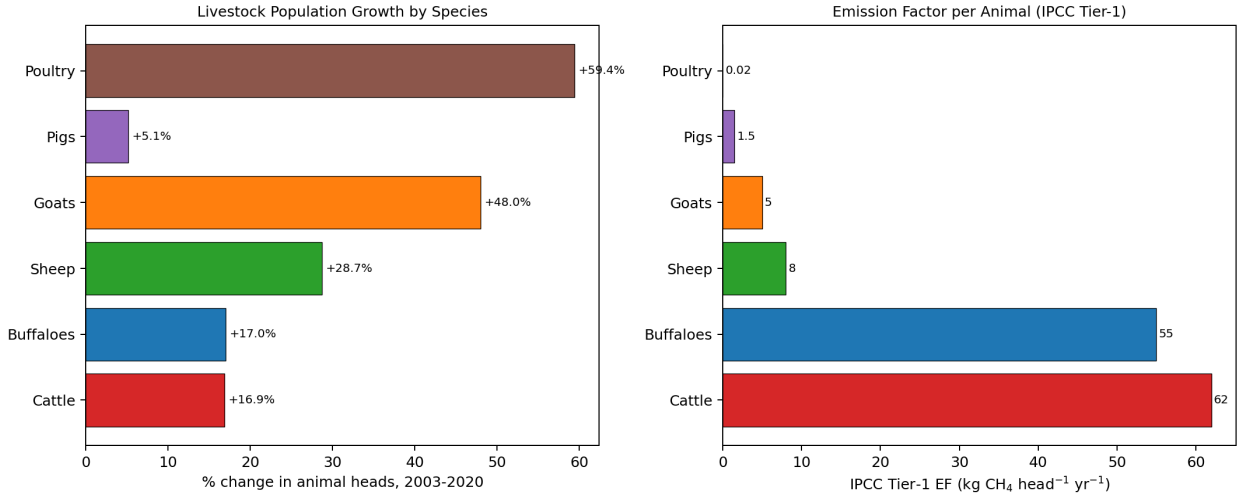
Figure A10 decomposes the growth in Tier 1 livestock methane into the contributions of the six species, and Figure A11 reports the proportional growth of each species. Cattle dominate the level, while goats and poultry grow fastest in proportional terms. These figures use the full grid, so their totals match Table A1.

Figure A10. Livestock methane by species, 2003 to 2020



Notes: Stacked Tier 1 methane by species. Source: AGLW with Tier 1 factors.

Figure A11. Proportional species growth

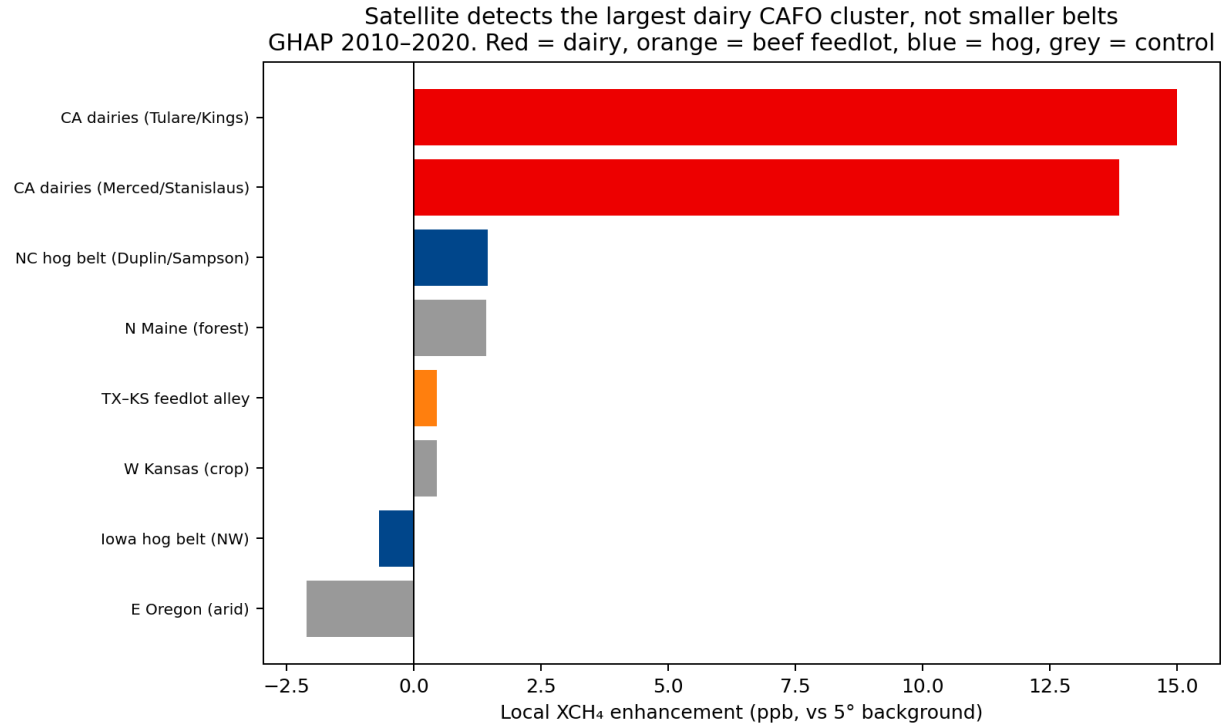


Notes: Head count growth by species, 2003 to 2020. Source: AGLW.

A6 Additional U.S. Validation

Figure A12 reports the local methane enhancement over each United States livestock region, showing that only the California dairy cluster clears the detection floor, and Figure A13 maps the enhancement over the contiguous United States with the major clusters marked.

Figure A12. Enhancement by United States livestock region



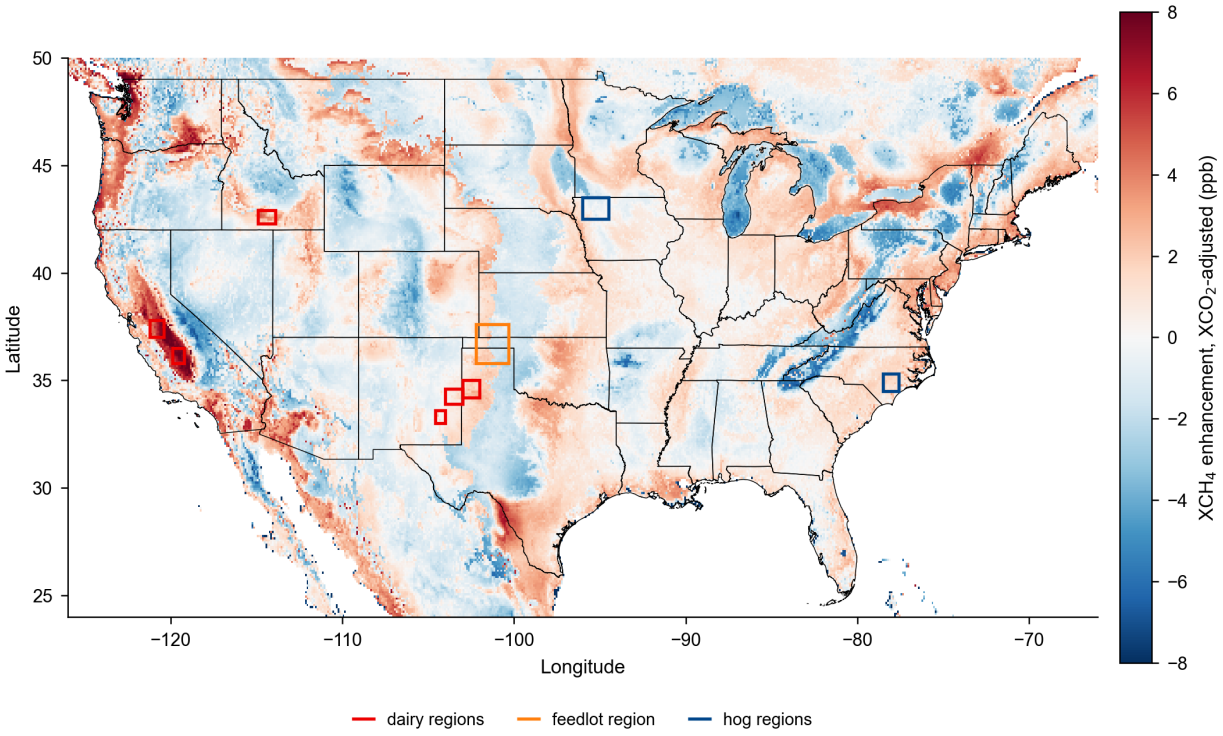
Notes: Local methane enhancement over dairy, beef, and hog clusters and rural controls. Source: GHAP.

Table A8. Satellite methane tracks the value of milk sold

	(1)	(2)	(3)	(4)
Log milk sales ($)	0.273*** (0.064)		0.096 (0.070)	−0.038 (0.121)
Log dairy cows		0.476*** (0.101)		0.521*** (0.180)
Log beef cattle			0.587*** (0.185)	

Notes: Raw satellite XCH_4 on log county quantities, 2° neighborhood fixed effects, standard errors clustered by neighborhood, 2017. Milk sales in dollars come from the Census of Agriculture. The sample is the 953 counties reporting milk sales, 25,208 grid cells. Milk revenue and the dairy herd are close to collinear, so column 4 cannot separate them and should not be read as evidence against revenue. $^{***}p < 0.01$. Source: GHAP and USDA NASS Census of Agriculture.

Figure A13. North America methane enhancement



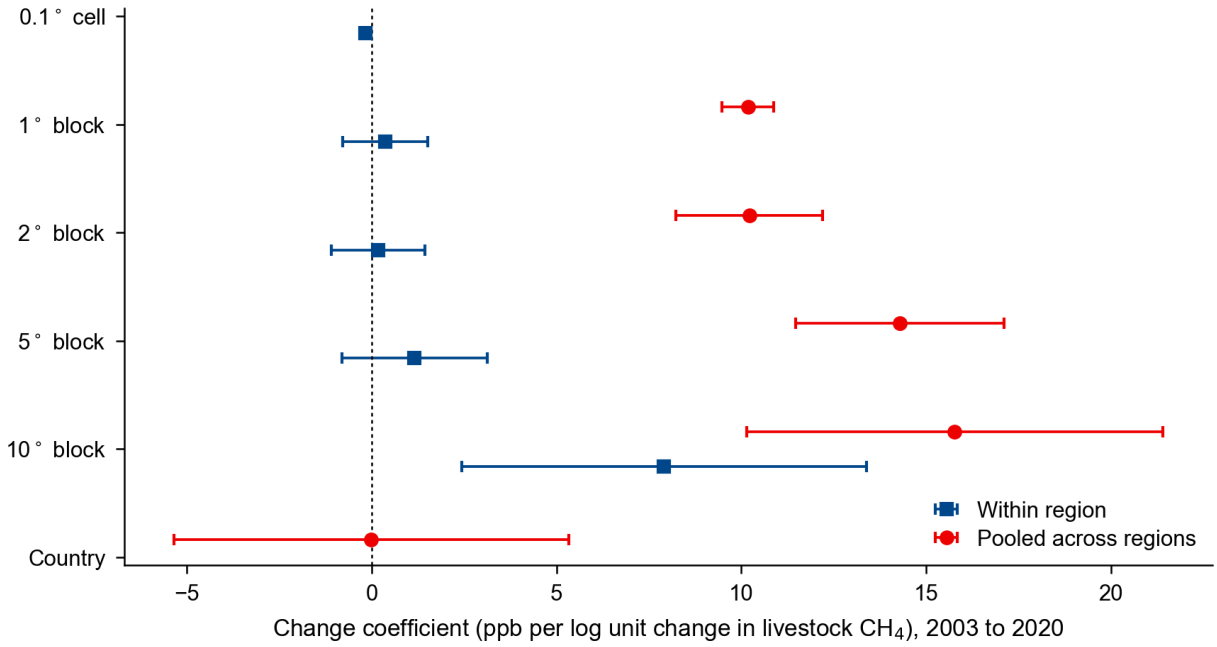
Notes: Local XCH_4 enhancement over the North America with livestock clusters marked. Source: GHAP.

Table A9. At county resolution, the relationship is positive, and the controls behave

	(1)	(2)	(3)	(4)	(5)	(6)
Log cattle	2.530***	2.075***	0.515***	0.527***		
	(0.294)	(0.238)	(0.134)	(0.122)		
Log dairy cows					0.425***	
					(0.088)	
Log milk sales ($)						0.256***
						(0.056)
Fossil (GFEI)	No	Yes	No	Yes	Yes	Yes
Waste (EDGAR)	No	Yes	No	Yes	Yes	Yes
Rice	No	Yes	No	Yes	Yes	Yes
2° neighborhood FE	No	No	Yes	Yes	Yes	Yes
Observations (cells)	50,547	50,547	50,547	50,547	50,547	25,208
R^2	0.155	0.344	0.027	0.128	0.132	0.140

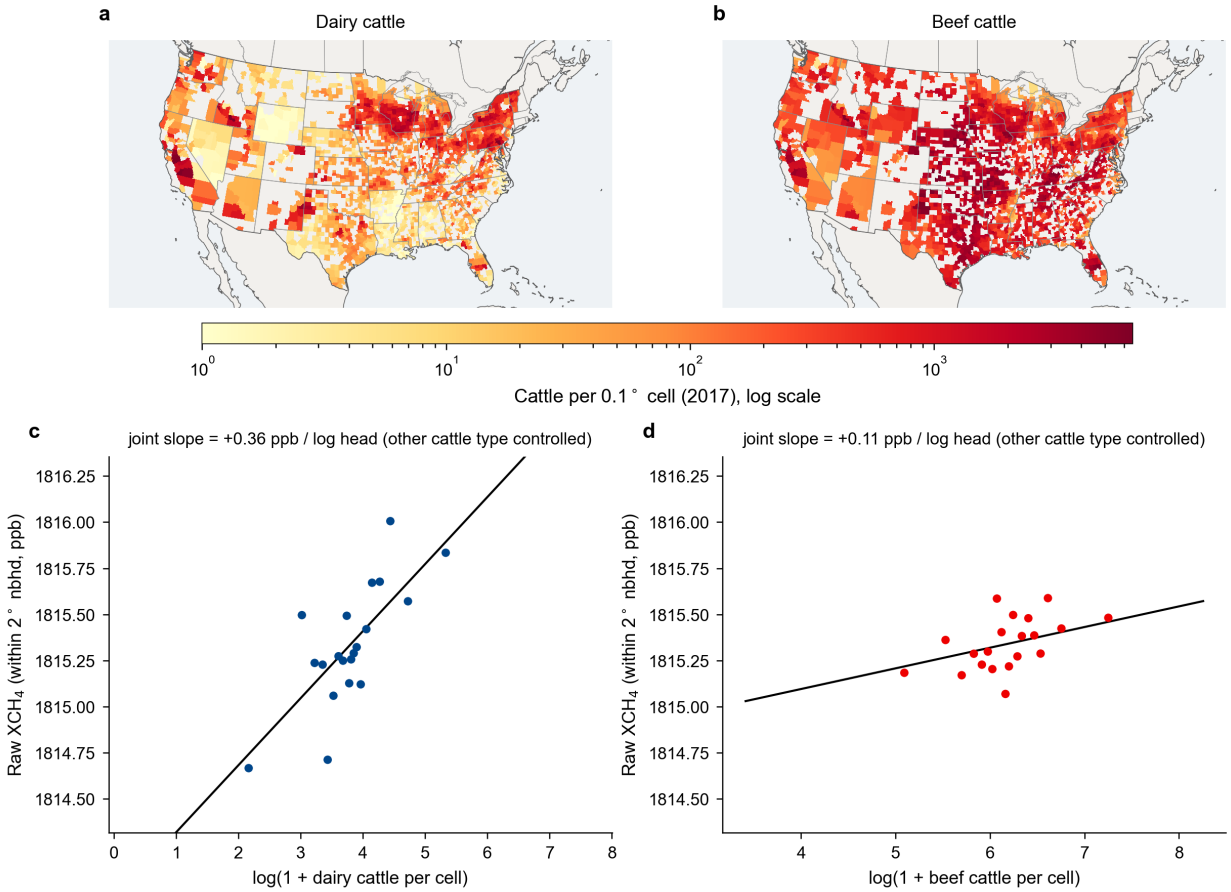
Notes: Column (6) replaces the animal count with the value of milk sold, so the estimate is an elasticity of the column with respect to farm revenue; it is estimated on the counties that report milk sales. The within neighborhood R^2 is small because cell-level column methane is dominated by transport and retrieval noise, which is why the identification rests on the coefficient rather than on fit. $^{***}p < 0.01$. Source: GHAP, GFEI, EDGAR v2025, GlobalRice20, USDA NASS Census of Agriculture 2017.

Figure A14. The satellite does not track change, at any level of aggregation



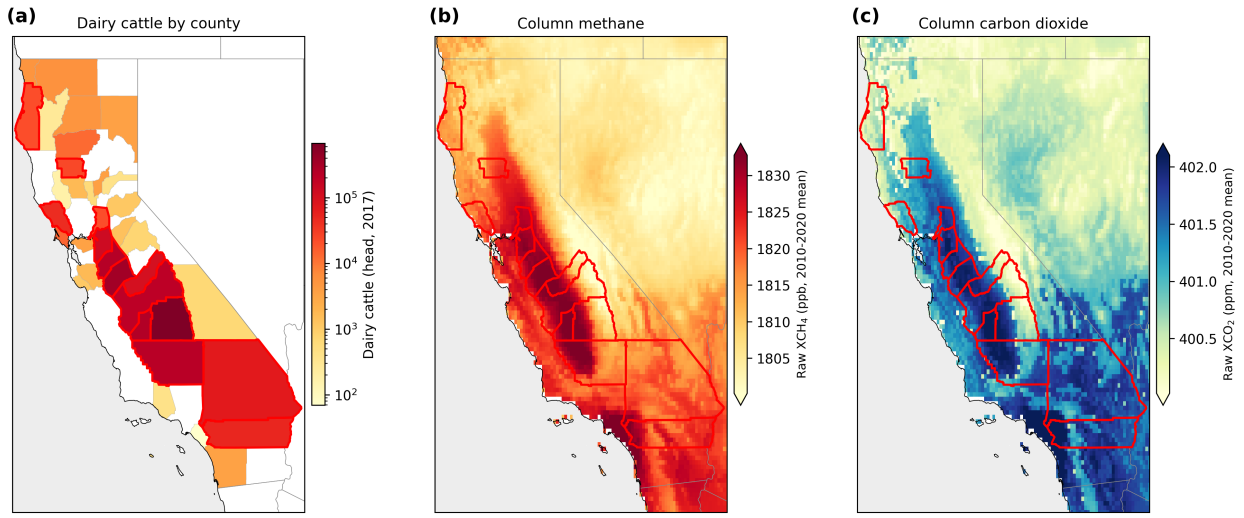
Notes: Change in raw XCH_4 on the change in log livestock methane, 2003 to 2020, by unit of aggregation. Red circles pool units across the world; blue squares compare units only with nearby units.Note: the large pooled coefficients reflect the coincidence that tropical regions grew both their herds and their methane fastest; within a region the coefficient is indistinguishable from zero everywhere except the coarsest block. Source: GHAP and AGLW.

Figure A15. Satellite methane tracks dairy, not beef



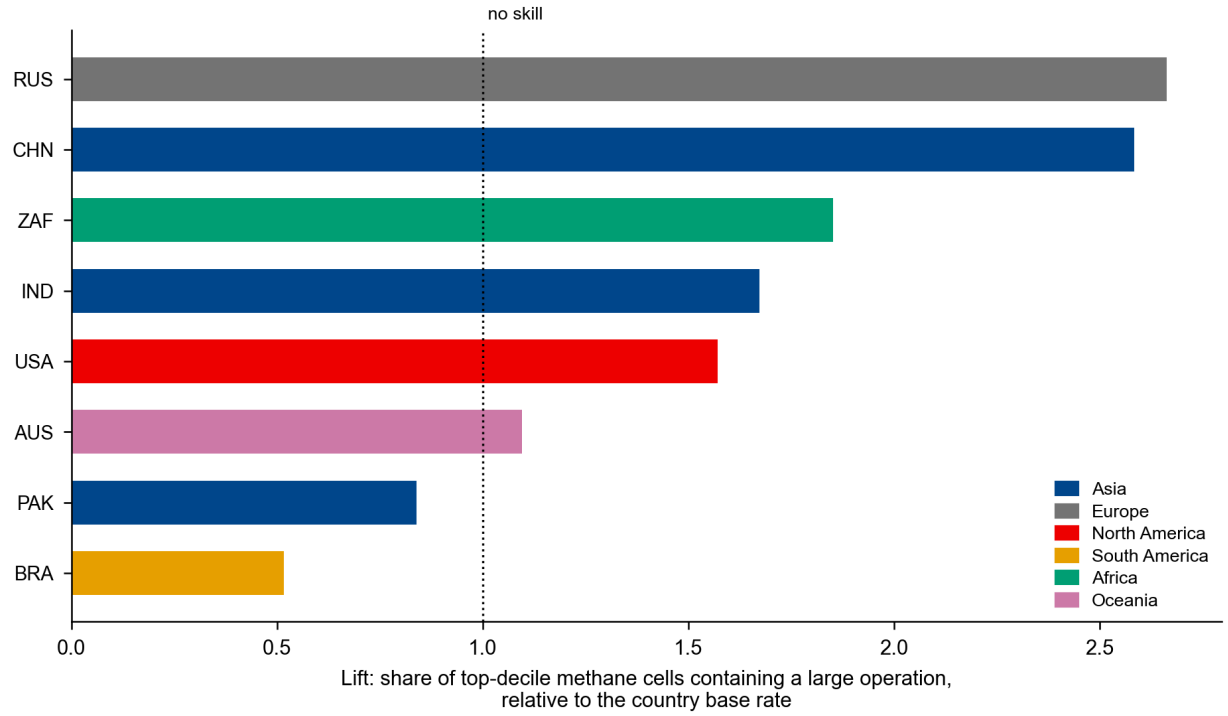
Notes: (a) Dairy and (b) beef cattle per 0.1° cell from the USDA county census, 2017, on a common log scale, so the two herds are directly comparable: beef is both denser and far more widely spread. (c) and (d) plot raw satellite XCH_4 against each cattle type after partialling out the neighborhood fixed effects *and the other cattle type*, so the plotted slope is the joint coefficient of Table 2, column (3). The two lower panels share a vertical scale; the dairy relationship slopes up while the beef relationship is flat. Source: GHAP and USDA NASS.

Figure A16. The California dairy cluster sits on the state methane maximum



Notes: (a) Dairy cattle by county, USDA 2017. (b) Raw satellite XCH_4 and (c) raw satellite XCO_2, GHAP 2010 to 2020 means in absolute units. The national top decile dairy counties are outlined in red in every panel. Source: GHAP and USDA NASS.

Figure A17. The detector against the global asset inventory



Notes: Share of each country's top decile of the within-neighborhood methane column that contains a large Climate TRACE cattle operation, 700 or more dairy or 1,000 or more beef head, relative to the country's base rate. Cells are the 2019 livestock cross section inside each country's asset envelope; countries shown have at least 30 target cells. Facilities are located from imagery and permits, never from methane, so the test is independent; inventory completeness differs by country, which is why lift is computed within country and never pooled. Russia's records carry Climate TRACE's lowest confidence grade. Source: Climate TRACE (Davitt et al., 2026), GHAP, AGLW.